유연인쇄전자학술지, 2023 년 0 월, 제 0 권 제 0 호, pp. 00-00
Journal of Flexible & Printed Electronics, Month 2023, Vol. 0, Issue 0
Received 2023-00-00, Revised 2023-00-00, Accepted 2023-00-00
https://doi.org/10.56767/jfpe.2022.0.0.00

REVIEW

Printed Graphene-based Interconnects and Vias for Flexible Hybrid Electronics

Ganapathi Bharathi[1], Seongin Hong[1,2,*]

[1]Department of Physics and Semiconductor Science, Gachon University, Seongnam 13120, Republic of Korea
[2]Department of Semiconductor Engineering, Gachon University, Seongnam 13120, Republic of Korea

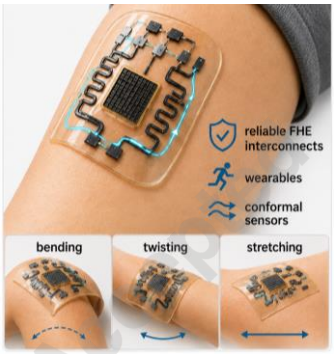

ABSTRACT (250 단어 이내)

Graphene-based inks are emerging as a mechanically resilient alternative to silver and copper nanoparticle systems for printed interconnects in flexible hybrid electronics (FHE). Unlike brittle metallic films, graphene flake networks survive repeated bending through crack bridging and percolation reconfiguration. However, the intrinsic-to-practical conductivity gap remains the central challenge: inter-flake junction resistance places printed film conductivity orders of magnitude below bulk metals. This review examines graphene ink formulation, covering liquid-phase exfoliated, electrochemically exfoliated, and reduced graphene oxide sources, along with inkjet, aerosol jet, screen printing, gravure printing and Electrohydrodynamic (EHD) printing strategies. Via formation, largely overlooked in existing literature, receives dedicated treatment covering sidewall coverage, aspect ratio constraints, and hybrid graphene–metal approaches. Conductivity enhancement routes, mechanical fatigue under cyclic bending, and integration with thinned silicon dies are also discussed. This review offers practical guidelines for ink selection, printing optimization, and via engineering in FHE.

Key Words: Graphene Ink, Graphene-metal hybrid inks, Printed Interconnects, Via Formation, Flexible Hybrid Electronics

*Correspondence: seongin@gachon.ac.kr

1. INTRODUCTION

The modern electronics industry is witnessing a profound paradigm shift as form factors transition from traditional rigid, rectangular geometries to complex, soft, and conformable architectures.[1] This evolution is driven by the need for devices that can interface seamlessly with biological surfaces, such as the human body, or wrap around irregular structures for structural health monitoring.[1] At the heart of this transition lies Flexible Hybrid Electronics (FHE), a technology that strategically combines the high-performance computation and communication capabilities of rigid silicon integrated circuits (ICs) with the scalability and mechanical compliance of printed circuitry.[1,2] As outlined in the NextFlex roadmap, this hybridization addresses the inherent trade-off between the high charge-carrier mobilities of monocrystalline silicon (~1000 $cm^2/V \cdot s$) and the low-cost, large-area manufacturability of solution-processed electronics.[1] The resulting systems, ranging from wearable health monitors and soft robotics to conformal Internet-of-Things (IoT) sensors, require a holistic approach to design that balances electronic performance with extreme mechanical durability.[1,2]

Despite the rapid progress in FHE, the interconnection network remains the critical weak link in system-level reliability.[2] Interconnects and vertical interconnection accesses (vias) must not only carry substantial current densities but also survive repeated bending, twisting, and stretching without catastrophic failure.[2,3] This is not merely a material-level selection problem; it is a system-level challenge involving thermo-mechanical coupling and significant mismatches in the coefficient of thermal expansion (CTE) and elastic modulus between rigid dies and flexible substrates.[2,4] To interface the micro-scale contact pads of thinned silicon dies with the macro-scale printed traces, complex redistribution layers (RDL) and fan-out structures are required.[1] These structures often serve as stress concentrators, where the transition from a rigid component (modulus ~100s of GPa) to a soft polymer substrate (modulus ~kPa to 180 GPa) induces high shear and normal stresses, leading to delamination and circuit breakage.[1,5,6]

Conventional solutions have relied heavily on silver (Ag) and copper (Cu) nanoparticle (NP) inks, yet these materials face inherent physical limitations. Ag nanoparticle inks, while dominating the market due to their high conductivity and oxidation resistance, are essentially brittle at the system level.[5,6] They typically exhibit channel cracking or grain boundary fracture at strains of less than 5%, which is insufficient for the dynamic 20–30% strain requirements of skin-wearable applications.[4,6] Furthermore, printed metallic tracks possess a porous microstructure that renders them highly susceptible to electromigration (EM) at high current densities. According to Black's equation, mass transport is accelerated along grain boundaries and interfaces, causing void formation at the cathode and aggregations (hillocks) at the anode, which eventually precipitates circuit breakdown.[4] Copper NP inks offer a lower-cost alternative but suffer from rapid oxidation under ambient conditions, forming insulating oxide layers (CuO_x) that drastically degrade electrical performance and necessitate complex, high-temperature sintering processes that are incompatible with low-thermal-budget plastic substrates like PET.[7,8]

Graphene, an atomically thin 2D honeycomb lattice of carbon atoms, has emerged as a formidable candidate to address these deficiencies.[9,10] From a condensed-matter physics perspective, graphene's charge carriers mimic relativistic particles, described by the Dirac equation as massless Dirac fermions, which enables high carrier mobilities (15,000–100,000 $cm^2/V \cdot s$) and near-ballistic transport.[10] Beyond its phenomenal electronic properties, graphene possesses intrinsic mechanical flexibility and exceptional strength, capable of sustaining elastic strains exceeding 20%—and in some forms, much higher—without loss of functionality.[9,11,12] Its chemical inertness provides stability against oxidation, while its unique structure prevents electromigration at moderate current densities, as the robust sp^2 hybridization of the carbon lattice resists the high electron flux that typically displaces atoms in metallic lattices.[8,11,12] Furthermore, graphene's conductivity can be precisely tuned through chemical doping or hybridization with

metallic fillers, which bridge flake-to-flake junctions and reduce contact resistance.[8,9] However, the integration of graphene into FHE faces a fundamental technical hurdle: the conductivity gap. While a pristine single layer of graphene is highly conductive, solution-processed printed graphene networks typically exhibit conductivities that are 10–100 times lower than bulk copper.[9,13] This discrepancy arises from the high resistance at the numerous flake-to-flake junctions within the percolating network, as well as the presence of insulating polymer residues from the ink formulation.[7,13] Navigating this "central tension"—maintaining graphene's mechanical superiority and chemical stability while pushing its conductivity toward metallic standards—is the core objective of current research and the primary focus of this review.

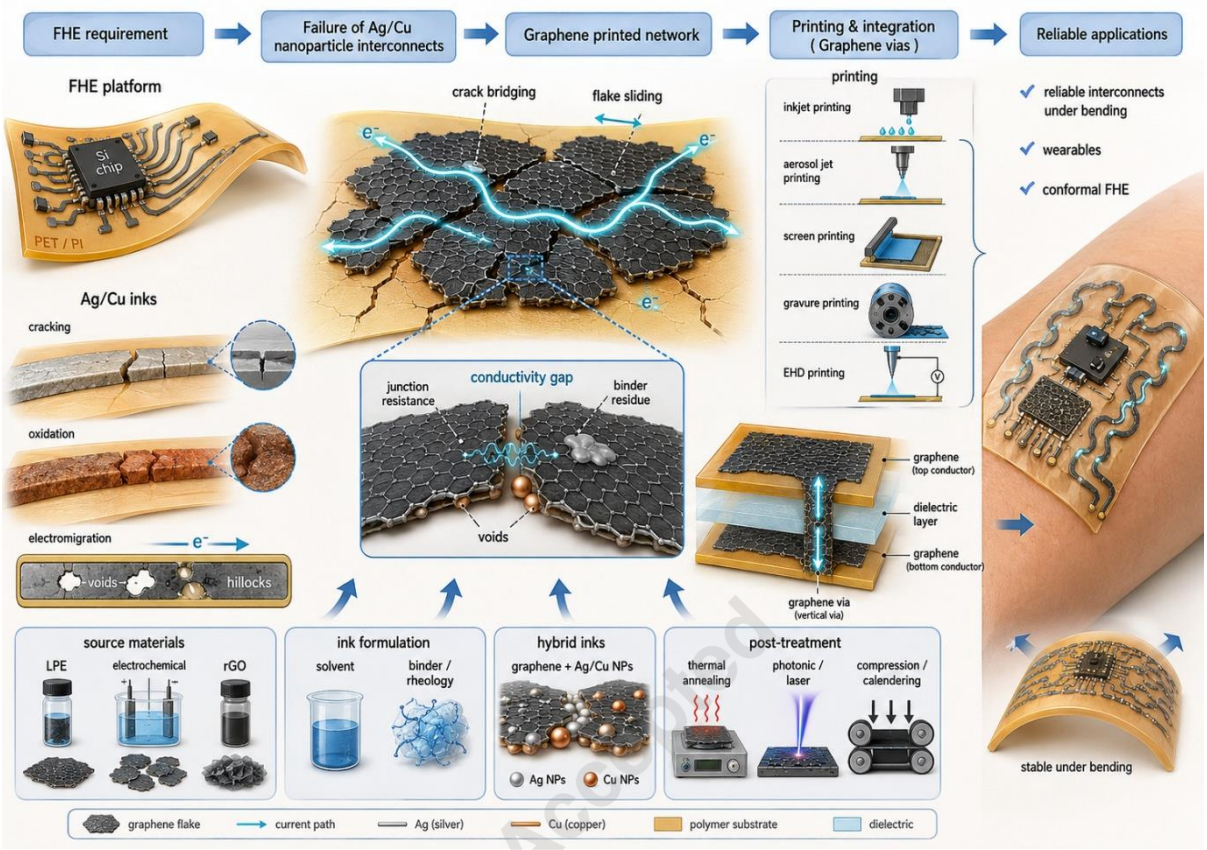

Fig. 1. Schematic overview of graphene-based interconnects and vias for flexible hybrid electronics, showing the transition from Ag/Cu interconnect failure to printed graphene networks, conductivity-gap mitigation strategies, printing/integration routes, and reliable wearable FHE applications.

Fig. 1 provides a schematic overview of this landscape, tracing the transition from Ag/Cu interconnect failure modes to printed graphene percolation networks, the conductivity-gap mitigation strategies discussed in this review, and the target FHE application space.

The discussion is organized around the practical demands of FHE interconnects rather than graphene's intrinsic properties. Starting from the electrical and mechanical requirements that define the design space, it moves through ink formulation — sources, solvents, hybrid systems — into printing method selection, and then into via formation, which receives detailed treatment because it remains the least developed part of the graphene interconnect literature. Conductivity enhancement and mechanical reliability close the discussion. Graphene's role here is strictly as a passive conductor; its behavior as a transistor channel, transparent electrode or sensing material is left aside, because the design questions are entirely different.

2. Graphene Inks for Printed Interconnects

2.1. Electrical and mechanical requirements

The performance criteria for the interconnects must be revisited when it comes to the FHE. In general, the interconnects in FHE have the role of either power distribution or signal routing. The power distribution interconnect lines should have the sheet resistance less than 1 ohm/sq, otherwise the circuits will face ohmic losses due to Joule heating effect. In the case of signal routing, the sheet resistance values can go upto 10 ohm/sq, since the signal integrity and timing margin are significant here.[14] Conventional printed/sintered copper-based interconnects set the benchmark of ~50 m.ohm/sq at 1 µm thickness, which is very low compared to the graphene interconnects. To close this gap in the performance, graphene interconnects should be optimized based on the sp^2 network density and multipass printing.[15–17] It is important to note that, unlike metal interconnects like Cu or Ag (bulk conductivity over 10^7 S/m), the conductivity in graphene is governed by the long-range ballistic transport within the graphene lattice and the inter-flake junction resistance/flake orientation/percolation pathway, when printed.[14,18,19]

Table 1. Comparison of major graphene source materials preparation routes for printed interconnect applications.

Preparation Method	Flake Size	Defect Density	Conductivity Range	Scalability	Suitable Applications	Ref
Liquid-Phase Exfoliation (LPE)	100–500 nm	Very low (pristine); I_D/I_G ratio typically ~0.17–0.28.	~1×10^4 to 5×10^4 S/m.	Highly scalable and cost-effective.	High-resolution inkjet and aerosol jet printing for TFTs and antennas.	[11, 20, 24]
Electrochemical Exfoliation (ECE)	1–10 µm.	Moderate; residual oxygen groups (C/O ~5–12) and I_D/I_G ~0.4–1.9.	Up to ~1×10^5 S/m for single sheets.	Scalable with fast production times.	Performance electrodes for organic field-effect transistors and supercapacitors.	[17, 25]
Hummers' method (Oxidative route)	0.7–100 µm.	High; residual oxygen and lattice vacancies persist post-reduction.	Typically, < 1×10^4 S/m; optimized films can reach upto ~8.5×10^4 S/m.	Most cost-effective and bulk-scalable.	Bulk deposition for chemical sensors, energy storage, and thick-film composites.	[19, 26, 27]

Note: The listed values are representative ranges and can vary with precursor quality, processing conditions, flake size, defect density, residual functional groups, binder content and post-treatment. Conductivity values refer to practical graphene films or printed structures, not intrinsic single-layer graphene.

Electromigration resistance is equally important to the current carrying capacity in FHE interconnects. At high current densities, the atomic migration takes place in the interconnects, which results in void formation and affects the circuit operations. This void formation is known as electromigration, and the metal nanoparticle-based inks are more susceptible to it. In addition, the thermal mismatch and mechanical strain can also cause degradation of metallic ink-based interconnects. Alternatively, graphene inks-based interconnects are highly resistive to electromigration effect, due to the strong covalent C=C bonds in the graphene backbone.[3,20,21]

The mechanical requirements of the interconnects vary based on the specific application. For conformal and flexible electronics, interconnects generally need to withstand moderate bending and strain levels up to approximately 5%. In wearable electronics, the requirement becomes stricter because the interconnects are repeatedly exposed to body motion, bending, twisting, and local stretching; therefore, strain tolerance above 10% is usually required, while high-motion regions such as fingers, elbows, and knees may impose substantially larger local strains.[22,23] Fully stretchable systems are more demanding than flexible FHE, since their reliability is governed mainly by cyclic tensile deformation rather than bending alone. Therefore, endurance over 10,000

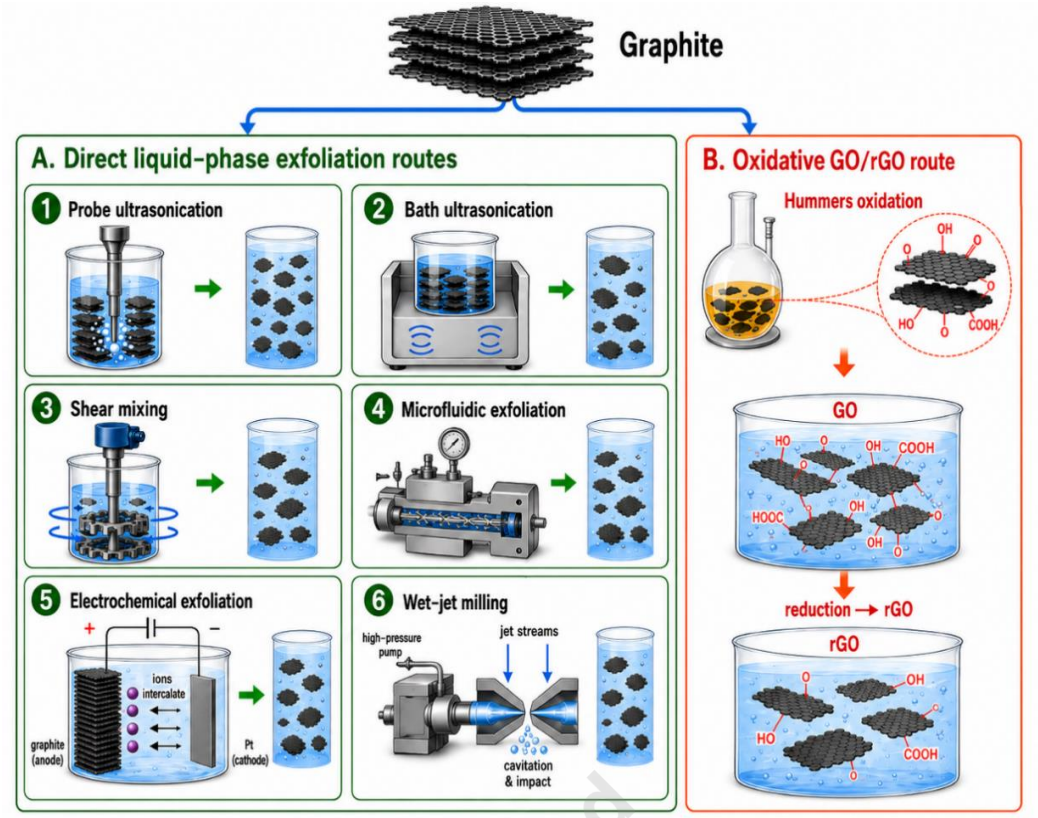

Fig. 2. Schematic representation of graphene production routes from graphite. Direct liquid-phase exfoliation methods include probe ultrasonication, bath ultrasonication, shear mixing, microfluidic exfoliation, electrochemical exfoliation, and wet-jet milling, where mechanical, acoustic, shear, hydraulic, or electrochemical forces overcome the interlayer van der Waals interactions in graphite to produce few-layer graphene dispersions. The oxidative route, shown separately, involves Hummers oxidation of graphite to graphene oxide (GO), followed by reduction to reduced graphene oxide (rGO), with higher dispersibility but increased oxygen functional groups and defect density.

bending cycles at a bending radius of 5 mm can be regarded as a useful baseline criterion for flexible and wearable interconnects, but not as a complete reliability criterion for stretchable systems.[16,24] For stretchable interconnects, cyclic stretch–release testing at the target strain level, together with resistance stability under deformation, is also necessary. The mechanical flexibility and high aspect ratio of graphene help to bridge the gaps created during strain-induced deformation. Stress in printed graphene interconnects can also be reduced by placing the conductive layer near the neutral mechanical plane of the multilayer stack.

The mechanical feasibility of the FHE interconnects is also governed by the adhesion of interconnects to flexible substrates, such as polyimide (PI), polyethylene terephthalate (PET), paper and textile. For better adhesion to these substrates the van der Waals forces and mechanical interlocking should work in combination.[8,18,21] More importantly, the surface tension of the conductive ink should match the surface energy of the substrate, which may require a surface treatment step. The native surface roughness of the target substrate also plays a role in adhesion, for example, the PI substrate with higher surface roughness can yield better adhesion than the PET substrate.

2.2. Graphene source materials

The choice of graphene source materials determines the morphology, electrical conductivity and processability of the interconnects. Among several preparation methods, liquid phase exfoliation (LPE) remains the most viable method to produce large quantities of graphene inks with negligible oxidation effects.[18,25,26] In LPE, the delamination of graphite into graphene sheets is achieved by ultrasonication or high-shear mixing.

One important point to note is the surface tension of the exfoliation solvent should match the surface energy (~40mN/m) to achieve maximum exfoliation efficiency. The typical size of graphene flakes ranges from 100-500 nm and thickness can be 2–3 nm (3–8 layers), depending upon the exfoliation duration.[17,20,27,28] In fact, it is the trade-off point, i.e., the higher the exfoliation duration the thinner the graphene sheets (reduced no. of layers), but with the compromise in the lateral size (leads to nanofragments) and defect density. The LPE graphene inks can produce interconnects with conductivity up to 1–5×10^4 S/m, post annealing. Electrical conductivities over ~10^5 S/m can be achieved in graphene inks prepared by electrochemical exfoliation (ECE).[13,28,29]

In the ECE protocol, the graphene source solution is prepared by electric current-assisted intercalation of organic/inorganic intercalants into graphite (rod/crystal/foil), followed by a mild sonication. The ECE process can produce graphene (1–5 layers) with large lateral size upto 10 um and lowest defect density. Graphene interconnects produced from the ECE graphene inks are suitable for high performance signal routing, however the electrolyte/intercalant removal and scalability challenges remain.[17,21]

Reduced graphene oxide (rGO) is the cheapest and highly scalable graphene source, produced by the oxidation of graphite by Hummers' method. In this process, graphite is oxidized into graphite oxide in the presence of harsh oxidizing agents followed by delamination into graphene oxide (GO).[19,30,31] The aqueous dispersibility of GO is excellent, suitable for high throughput printing. The bottleneck with GO is the presence of sp^3 hybridized carbon and large amount of oxygen functional groups caused by the Hummers' oxidation process. A post-synthesis reduction step (chemical/thermal/photonic) can greatly reduce the oxygen moieties and restore the sp^2 hybridization in the graphene lattice to some extent. The graphene source after this reduction step is known as rGO.[11,19] Though the conductivity of rGO cannot match the LPE or ECE graphene, it is suitable for thick film applications processed by bulk deposition. It's further important to note that, there is a persistent gap between the intrinsic and practical conductivities of graphene. Fig. 2 summarizes the principal graphene production routes from graphite: the direct liquid-phase exfoliation family (probe sonication, shear mixing, electrochemical, wet-jet milling) and the oxidative GO/rGO pathway, each carrying distinct trade-offs in defect density and dispersibility.

The key differences among these graphene preparation routes are summarized in Table 1. In general, LPE provides low-defect pristine graphene flakes with moderate conductivity and good compatibility with inkjet and aerosol jet printing. ECE can produce larger flakes with higher electrical performance, but electrolyte removal and process control remain important considerations. In contrast, the oxidative GO/rGO route offers the highest scalability and aqueous processability, although the residual oxygen groups and lattice defects limit the final conductivity. Therefore, the selection of graphene source material should be made based on the required balance between conductivity, defect density, ink stability, printability and production scale.

The single pristine graphene can reach electrical conductivity over ~10^5 S/m, but when it comes to the printed interconnects the macroscopic conductivity is dominated by the inter-flake junction resistance.[11,18] An electron in graphene has to navigate through the disordered network, where the tunneling resistance at flake-flake overlap acts as a primary bottleneck. This gap can be narrowed down by maximizing the flake alignment and packaging density.

2.3. Solvent systems and binders

Graphene ink formulation requires a balance between ink rheology and thermodynamic stability. The ink formulation process takes place in two major steps, first, exfoliation of graphite using a single or combination of solvents and stabilizers, and then ink preparation with a suitable solvent, binders and additives.

The choice of exfoliation solvents includes N-Methyl-2-pyrrolidone (NMP), dimethylformamide (DMF), ethanol, isopropyl alcohol (IPA)/water, etc. Among these, NMP and DMF are widely used solvents because their surface tension values (~40 mN/m) and Hansen solubility parameters closely match those of graphitic materials. The Hansen solubility parameters are commonly expressed as δ_D, δ_P,

and δ_H, corresponding to the dispersion-force, polar-interaction, and hydrogen-bonding components, respectively. For example, DMF has representative values of $\delta_D \sim 18.0$, $\delta_P \sim 9.3$, and $\delta_H \sim 7.7$ $MPa^{0.5}$, which provide good affinity toward the graphitic lattice.[26,32] NMP and DMF are effective, but problematic solvents because of reproductive toxicity and increasingly strict REACH/EU regulatory restrictions. Other solvents such as ethanol or IPA/water require stabilizers, such as ethyl cellulose or PVP to keep the exfoliated graphene stable, i.e., to contain reaggregation.[8,25,26]

Cyrene™ (dihydrolevoglucosenone), a cellulose derivative, has now been established as a potential 'green' solvent for graphite exfoliation. With better Hansen solubility parameters than NMP, Cyrene exhibits superior affinity to graphene. Cyrene can also serve as an additive to aqueous inks, since its higher viscosity (~14.5 mPa.s) can help to modify the ink rheology and printability.[25,26]

In the ink preparation step, the exfoliated graphene solution is transferred to a solvent-binder-additive system in order to achieve the printing rheology. The choice of solvent and binder systems is chosen based on the target substrate and thermal budget. If the substrate can withstand annealing temperatures over 350°C, cyclohexanone solvent with terpinol additive and ethyl cellulose binder is gold standard. Some cases used terpinol, ethyl lactate, ethylene glycol, and propylene glycol as standalone or in combination.[20,29,33] Aqueous graphene inks are prepared and used for substrates that require low-temperature processing. For such cases, surfactants like SDS or Triton X-100 are used to maintain graphene stability.[18,30]

The fluid mechanics of the inks remain distinct for different printing methods, and it is extremely important to optimize the ink properties accordingly. The widely used inkjet printing requires graphene inks with viscosity 1–20 mPa.s, and inverse Ohnesorge number (Z) between 1 to 14, in order to ensure stable jetting behavior, controlled droplet breakup, and suppression of satellite droplet formation.[15,21] The printability parameter or the inverse ohnesurge:

$$Z = \frac{1}{Oh} = \frac{\sqrt{\rho\gamma a}}{\eta}$$

Where, η = viscosity, ρ = density, γ = surface tension, and a = nozzle diameter

Aerosol jet printing accepts a wider viscosity window than inkjet, but the usable range depends strongly on atomization mode: ultrasonic atomization is typically limited to low-viscosity inks, whereas pneumatic atomization can process substantially higher-viscosity formulations. In contrast, screen printing employs paste-like inks with highest viscosity (few hundreds to few thousands of mPa.s) and shear-thinning characteristics, owing to the fundamentally different printing process.

2.4. Graphene/metal nanoparticle hybrid inks

The complementary limitations of metal nanoparticle inks and graphene inks have driven the development of hybrid inks, where metallic fillers improve the electrical conductivity of graphene networks while graphene helps retain mechanical flexibility and chemical stability. Among different combinations, graphene/Ag and graphene/Cu hybrid inks are the most representative systems for printed interconnect applications. Graphene/Ag inks mainly target high conductivity and oxidation-resistant interconnects, whereas graphene/Cu inks aim to reduce material cost while using graphene as a protective and conductive framework to suppress Cu oxidation. Therefore, both systems are discussed below in terms of their conductivity enhancement mechanism, mechanical reliability and formulation limitations.

Graphene/Ag composite inks

Ag is known for its exceptional electrical conductivity (~6.3×10^7 S/m) and better oxidation resistance, compared to other printable metals such as Cu.[7,34] When hybridized with graphene flake network, Ag metal nanoparticles establish a highly conductive pathway within the graphene flake network to boost the overall electrical conductivity of the printed lines. Parallelly, the graphene flake network surrounding the Ag nanoparticles thereby bridges the possible mechanical microcracks and connects the voids within. Furthermore, the interconnect lines printed with Ag-only inks suffer from the electromigration effects at high current densities. This effect is greatly suppressed when Ag-nanoparticles are hybridized with graphene, as the latter act as a matrix to hold the Ag nanoparticles and ensure long term conductive stability.[16,35]

Graphene/Cu inks

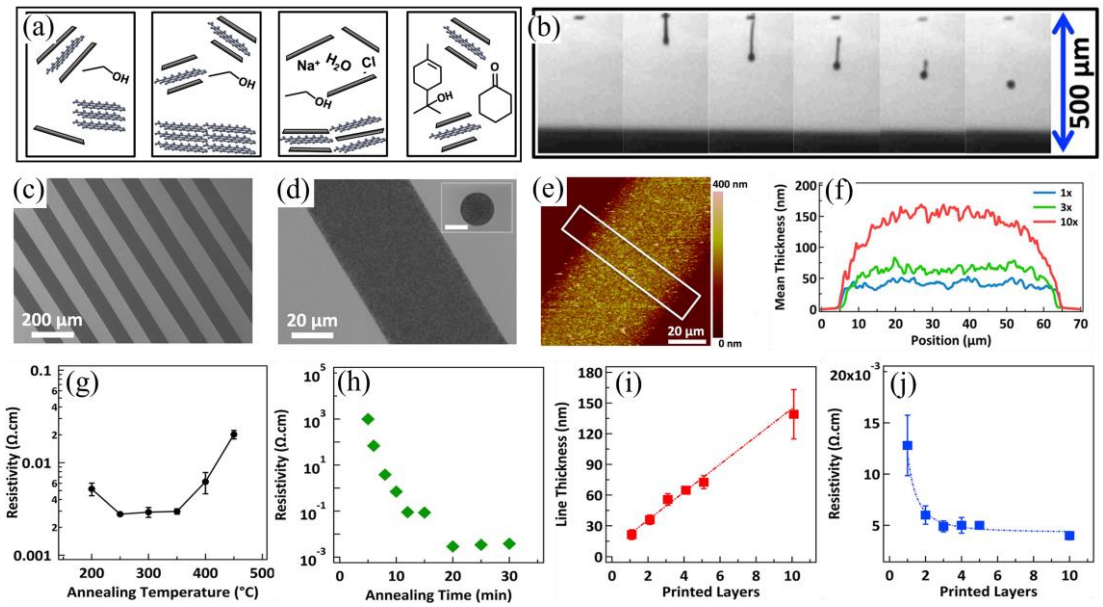

Fig. 3. Graphene ink preparation for inkjet printing and characterization of printed lines (a) Schematic illustration of the ink preparation method – Graphene exfoliation from graphite powder in ethanol/EC by probe ultrasonication, centrifugation-based sedimentation to remove residual large graphite flakes, salt-induced flocculation of graphene/EC, and final ink for inkjet printing is prepared by dispersion of the graphene/EC powder in 85:15 cyclohexanone/terpineol. (b) drop formation sequence for inkjet printing, with spherical drops forming after ~300 µm. Morphology of inkjet-printed graphene features on HMDS-treated Si/SiO_2. Scanning electron micrographs of (c) multiple printed lines and (d) a single printed line and drop (inset, scale bar corresponds to 40 µm) illustrate the uniformity of the printed features. (e) An atomic force microscopy (AFM) image of a single line following 10 printing passes that shows no coffee ring features. (f) Averaged cross-sectional profiles of printed lines after 1, 3, and 10 printing passes, which demonstrate the reliable increase in thickness obtained after multiple printing passes. The cross-sectional profiles are obtained from the averaged AFM height profile over ~20 µm as indicated by the boxed region in (e). Electrical characterization of graphene features. (g) Electrical resistivity of blade-coated films plotted against the annealing temperature for a fixed annealing time of 30 min, showing effective binder decomposition at 250°C and increased resistivity due to graphene oxidation above 400°C. (h) Dependence of electrical resistivity on the annealing time for a fixed annealing temperature of 250°C, showing that low resistivity is achieved following annealing for 20 min. (i) Thickness of inkjet-printed graphene lines on HMDS-treated Si/SiO_2 for increasing numbers of printing passes. (j) Electrical resistivity of the printed features for increasing numbers of printing passes, showing relatively stable performance after only three printing passes. Adapted with permission from [13]. Copyright © 2013 American Chemical Society

Cu can reach the bulk electrical conductivity nearly equal (~5.9×10^7 S/m) to Ag, at substantially lower material cost compared to Ag.[7,16,34,36,37] However, the major bottleneck is the oxidation susceptibility of Cu nanoparticles. Even at ambient conditions, Cu NPs can react with oxygen and form a poorly conductive Cu_2O/CuO surface layers. In the formulation of Graphene/Cu hybrid inks, graphene (or rGO) flake network can encapsulate the Cu NPs and act as a diffusion barrier for oxygen to reach Cu nanoparticles. This protective framework helps in preserving the Cu metallic core, which in turn improves the overall electrical stability and conductivity.[20,38]

The electrical performance and mechanical reliability of the interconnects printed using these graphene/metal hybrid inks is governed by the conductivity-flexibility trade-off. In general, increased metal loading can increase electrical conductivity by improving conductive percolation; however, excessive loading can lead to metal nanoparticle aggregation and rapid sedimentation.[16,39] Such aggregation of metal

nanoparticles results in poor printability of the inks and produces brittle interconnects. When maintaining a balance in the graphene-metal nanoparticle ratio, graphene flakes can act as a mechanical scaffold and maintain the durability of the metallic core, while retaining the percolative pathways during deformations.

3. Printing Techniques for Graphene Interconnects

Graphene can be used in flexible hybrid electronics (FHE), to create electrically functional patterns deposited with geometric precision, reliability, and speed. While conventional subtractive microfabrication uses harsh chemicals and high thermal budget processing steps, which are incompatible with polymer substrates like PET and PEN. In contrast, the additive printing techniques offer a low-cost, maskless, and digitally reconfigurable alternative for fabricating flexible electronic architectures.[20,40,41] The printed interconnect applications require a balance between high spatial resolution (for dense signal routing) and sufficient film thickness (for low-resistance power delivery).[42]

3.1 Inkjet Printing

Inkjet printing has emerged as a widely adopted method for printing complex device layouts and multilayer electronic architectures with high material utilization efficiency. In particular, the piezoelectric drop-on-demand (DOD) variant has been outstanding for graphene-based electronics due to its ability to produce precise microscale patterns while accommodating broad range of ink formulations.[15,43]

3.1.1 Resolution and waveform optimization

The resolution of patterns printed by inkjet printing is determined by the droplet volume (1-10 pL) and the wetting behavior of the substrate. The typical printing resolution of a DOD inkjet printer is reportedly 30-50 µm, and in some cases, it can go upto 20 µm line width upon careful optimization of the ink rheology, substrate surface energy, and printing parameters.[27,41,43] Interestingly, ejection of single spherical droplets can be achieved by tuning the piezoelectric actuation waveform, particularly the pulse rise and fall times, which can eventually minimize the formation of satellite droplets.

3.1.2 Physics of coffee-ring effect and mitigation

In the inkjet printing process, the primary challenge to be addressed is the coffee-ring effect, which results in non-uniform and ring-like printed patterns. It is a hydrodynamic phenomenon that originates from rapid solvent evaporation, where outward capillary flow transports the suspended graphene flakes toward the pinned contact line during droplet drying.[27,44,45] For graphene inks, coffee-ring suppression is usually achieved by controlling the internal flow of the droplet, the evaporation rate, and the ink–substrate wetting behavior. Therefore, the main mitigation strategies can be grouped into three approaches: Marangoni-flow engineering, substrate-temperature control, and substrate-wettability modification.

Marangoni flow engineering

The first strategy to mitigate the Coffee-ring effect is, creating an inward flow within the printed droplet to counteract the outward capillary flow. This inward flow is known as Marangoni flow, and it can be created by the surface tension gradients that originate when using the binary or ternary solvent systems such as cyclohexanone and terpinol.[13,20,46] The Marangoni flow helps to homogenize the suspended flakes/particles in the printed ink droplet.

Substrate temperature control

During the printing process, increasing the platen temperature (for e.g., 40 to 100°C) can accelerate the solvent evaporation, which in turn can ‘freeze’ the flakes and droplet geometry.[45,46]

Wettability modification

Another important strategy is the modification of the substrate wettability. The substrates with high wettability behavior will cause the spreading of printed droplets thereby increasing the possibility of coffee-ring effect. In contrast, when substrate wettability is decreased using coatings like HMDS, the droplet spreading is constrained and therefore the target printing geometry is maintained.[27,47]

3.1.3 Multipass strategies and clogging

The low solid loading of inkjet inks is a major limitation for conductive interconnects. Graphene concentration is usually kept below 1–

2 wt% to avoid nozzle clogging and unstable jetting.[43,48,49] Therefore, multipass printing is required to build thickness and reduce sheet resistance. In general, thickness increases with the number of passes and sheet resistance decreases.[17,28]

nozzle requires inks with graphene flake size below 400 nm (roughly).[11,15,27] This requirement improves printability, but it also increases junction resistance because smaller flakes create more boundaries. Fig. 3 shows a representative example of inkjet-printed

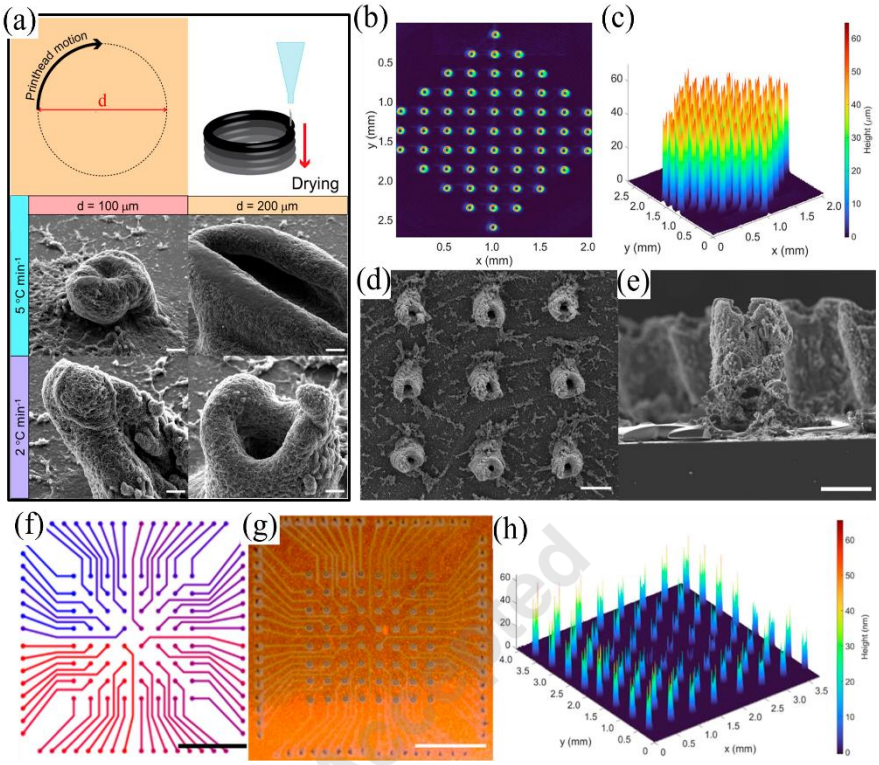

Fig. 4. 2.5 D printing of vertical interconnects. (a) top panel shows the Operational schematic representing additive manufacturing of carbon-based pillar structures and bottom panel shows SEM images of 2.5D pillar structures with different diameters, 100 and 200 µm, and postprocessed with different heating rates, 2 and 5 °C min^{-1}. All samples were printed on a silicon chip and fabricated using the quaternary formulation to leverage the glycerol-induced gelation of the deposited material. Scale bars are 20 µm for all SEM images. (b) Top view optical profilometry image of a 2.5D pillar structure array integrated onto a planar electrode and (c) its corresponding surface plot. (d) Top-down SEM photograph of a graphene sample with 2.5D pillar structures, scale bar 100 µm, and (e) its corresponding cross-sectional image, scale bar 50 µm. Both samples were printed on Kapton. (f) Toolpath used for the manufacturing of the electrode array, (g) the respective processed graphene sample printed on Kapton, and (h) its surface profile. Scale bar 2 mm for (f,g). Adapted with permission from [52]. Copyright © 2023 American Chemical Society.

However, too many passes increase processing time, solvent accumulation and the risk of re-dissolving the previous layer. One important point to note is that the graphene flake size must also be controlled to avoid clogging of ink particles at the nozzle. A practical rule is that the graphene flake size should be less than 1/50th of the nozzle diameter. For example, a 20 µm

graphene interconnect formation using an ethyl cellulose-stabilized graphene ink. Fig. 3a first describes the complete ink preparation route, where graphite is exfoliated in ethanol/ethyl cellulose by probe ultrasonication, followed by centrifugation to remove large graphite residues, salt-induced flocculation of graphene/ethyl cellulose, and final redispersion in a cyclohexanone/terpineol solvent mixture suitable

for inkjet printing. Fig. 3b confirms the droplet ejection behavior, showing that stable and nearly spherical droplets are formed after travelling a short distance from the nozzle. The printed-line morphology is then shown in Fig. 3c–e, where SEM and AFM images confirm that uniform graphene features can be obtained without severe coffee-ring formation. The cross-sectional profiles in Fig. 3f further show that the printed thickness increases systematically with the number of printing passes, which is important for reducing sheet resistance. The electrical data in Fig. 3g–j connect this morphological evolution with the post-processing condition, showing that annealing temperature, annealing time and multipass deposition strongly affect the final resistivity of the printed graphene lines. Therefore, Fig. 3 highlights that ink formulation, droplet stability, multipass printing and thermal annealing must be optimized together to obtain reliable graphene interconnects by inkjet printing.[13]

Recent inkjet-printed graphene interconnects have shown conductivities around 2.5×10^4 S/m using pristine graphene/EC inks,[28,49] while water-based electrochemically exfoliated graphene inks have reached around 3.91×10^4 S/m at approximately 50 µm resolution.[17] These values are useful, but still not metal-like. Inkjet printing is therefore more suitable for signal lines, sensors and moderate-current interconnects than for thick power buses.

3.2 Aerosol jet printing (AJP)

Aerosol jet printing (AJP) is a compelling alternative to inkjet printing, which is more suitable when fine features, high aspect ratio structures or conformal printing over uneven surfaces are required. In AJP, the ink is atomized into small droplets, typically 1–5 µm, and the aerosol stream is focused using a coaxial sheath gas.[20,42,50] This aerodynamic focusing allows a stand-off distance of 1–5 mm, which is a clear advantage over inkjet printing where the nozzle must remain close to the substrate.[40,51,52] Therefore, AJP can print over 3D surfaces, step edges and partially assembled electronic structures. In addition, AJP accommodates a significantly wider viscosity window (1–1000 cP), allowing the use of more concentrated, stable graphene dispersions. This is important because higher solid loading helps to build thickness faster and reduce sheet resistance. AJP is particularly useful for fine-pitch interconnects between rigid chips and flexible substrates, where conventional wire bonding is not suitable. It can also print 2.5D structures such as micropillars with aspect ratios upto 10.[52] This is where AJP becomes more than a planar printing tool. Fig. 4 shows the capability of aerosol-based printing to move beyond planar graphene lines and form 2.5D carbon interconnect structures. Fig. 4a presents the basic additive manufacturing route for carbon pillar formation, where controlled deposition and post-processing are used to build vertical structures with defined diameters. The SEM images in the same panel show that the pillar morphology depends strongly on the printing diameter and heating rate, indicating that solvent removal and structural consolidation are critical for maintaining vertical geometry. Fig. 4b and c further confirm the formation of an ordered pillar array on a planar electrode using optical profilometry, where the surface map verifies both the height profile and spatial uniformity of the printed structures. Fig. 4d and e show the top-view and cross-sectional SEM images of graphene pillar structures printed on Kapton, confirming that such 2.5D features can also be fabricated on flexible substrates. Finally, Fig. 4f–h connect the designed toolpath with the printed electrode array and its corresponding surface profile, showing how the printing path controls the final three-dimensional interconnect geometry. Therefore, Fig. 4 supports the point that aerosol-based printing is useful not only for fine planar interconnects, but also for localized vertical structures and chip-to-flex interconnection schemes in FHE.

3.2.1 Resolution overspray and edge roughness

The resolution of AJP printed patterns is governed by the focusing ratio (FR), which is given by the ratio between sheath gas and carrier

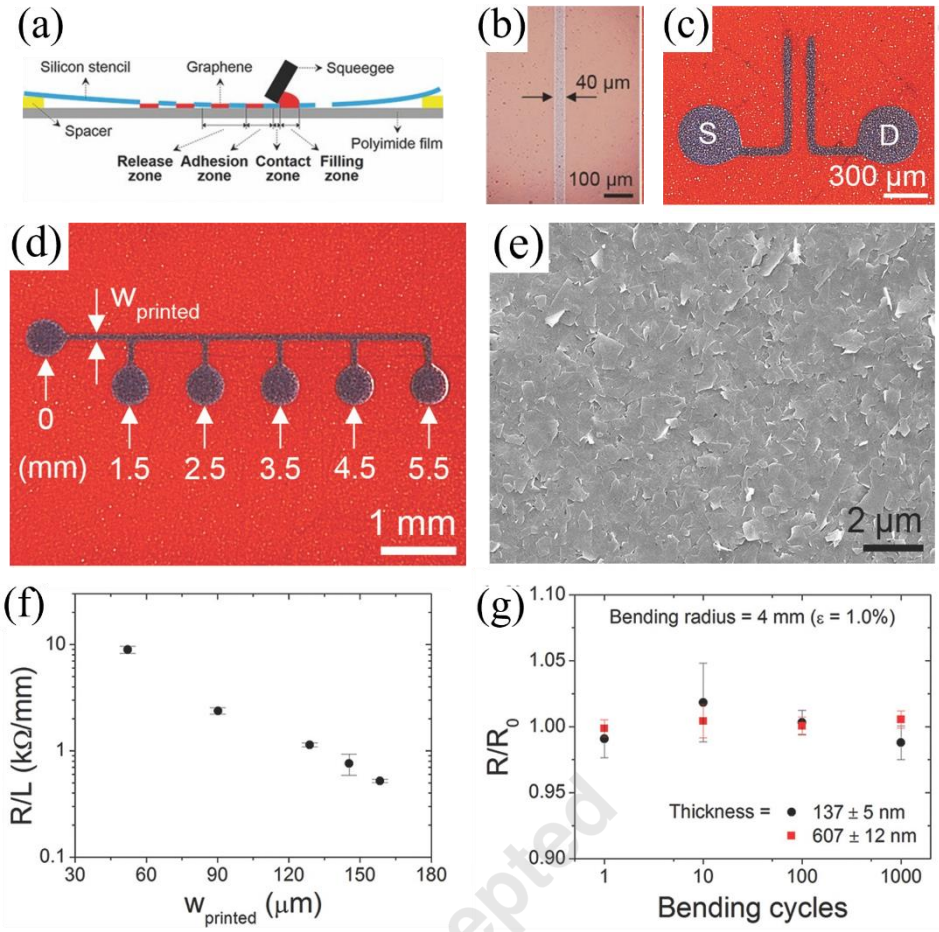

Fig. 5. Schematic illustration of screen printing and characterization of printing electrodes. a) Cross-sectional illustration of the screen printing method with the flexible silicon stencil during printing. b) OM images of a screen-printed graphene line with $w_{printed}$ of 40 μm. c) OM image of screen-printed graphene source and drain electrodes on a polyimide substrate for EGTs (W/L = 900 μm/90 μm). d) OM image of screen-printed graphene to measure electrical properties of the graphene lines for different lengths and $w_{printed}$. e) Scanning electron microscopy image of the graphene after annealing at a temperature of 300°C for 30 min. f) Resistance per unit length of the graphene as a function of $w_{printed}$. g) Relative resistance of the screen-printed graphene lines on flexible substrates with two different thicknesses over 1000 bending cycles at a bending radius of 4 mm, corresponding to 1.0% tensile strain. Adapted with permission from [57]. Copyright © 1999-2026 John Wiley & Sons, Inc.

gas. With appropriate focusing line widths of 10–20 μm can be achieved, and in some cases sub-10 μm lines are also reported.[18,20,42,50] However, there are a few drawbacks for AJP; Overspray – during the printing process, small, low inertia droplets escape from the main jet and deposit as sparse satellite spray. This eventually increases the effective line width of the printed pattern beyond the designed limit. One effective way to mitigate this is to saturate the sheath gas with solvent vapor, which in turn reduces the solvent evaporation on the flight and suppresses the overspray. Another bottleneck is the line edge roughness, which can be fixed by optimizing the printing parameters in practice.[40,51,53]

3.3 Screen printing

Screen printing is the practical workhorse for high-throughput printing of thick power interconnects, ground planes and large-area electrodes. Its main strength is that it can deposit thick films, usually 5–20 μm, in a single pass.[54–56] This makes it more suitable than inkjet printing when the aim is low resistance rather than fine resolution. The method is also compatible with roll-to-roll processing, which is

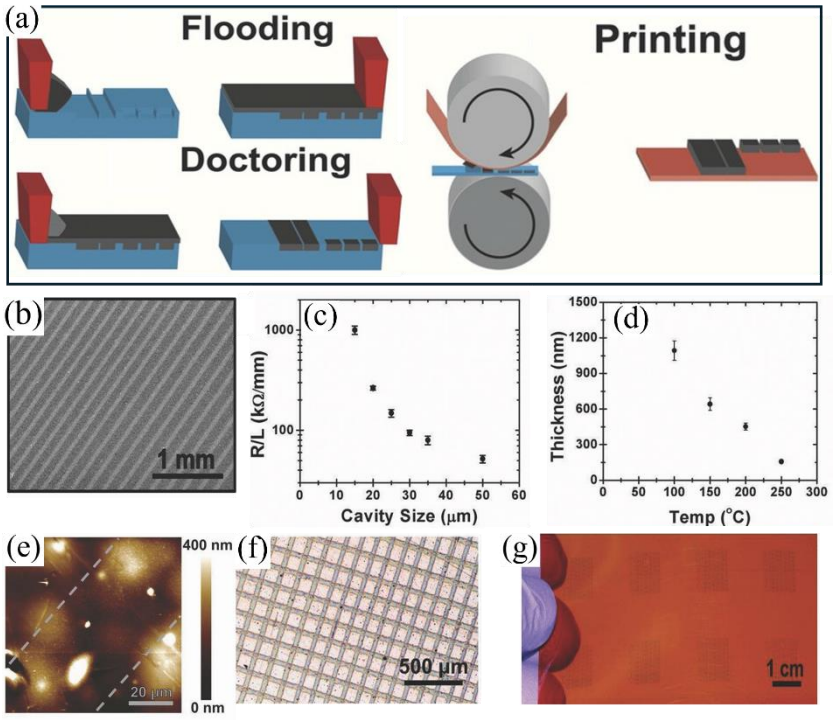

Fig. 6. Schematic illustration of gravure printing process and characterization of printed pattern; (a) illustration of the gravure printing method decomposed into three steps: flooding of the gravure cells; doctor blading; and printing. (b) microscopic image of the printed pattern. (c) Line resistance for the varying cavity size. (d) Thickness contraction during annealing for the graphene-EC composite. (e) AFM images of a printed line, illustrating that the printed lines are considerably thinner than the substrate surface roughness. (f) Printed crossbar array. (g) Photograph of large-area patterns. Adapted with permission from [29]. Copyright © 1999-2026 John Wiley & Sons, Inc.

important for industrial production of flexible circuits.

The limitation of screen printing is the resolution of printable pattern. Conventional screen printing usually gives line widths around 50–100 μm, which is mainly due to mesh geometry, paste spreading and stencil limitations.[56] This is not enough for fine-pitch signal routing, but acceptable for power tracks and robust interconnect lines. High-resolution stencils can push the feature size close to 40 μm, but this requires tighter control over paste rheology and printing pressure.[57]

Graphene screen-printing inks are fundamentally different from inkjet inks. They are high-viscosity, shear-thinning pastes, typically in the range of 1–10 Pa·s at moderate shear rate.[56,57] During printing, the paste must flow under the squeegee pressure and pass through the mesh. After deposition, it must rapidly recover viscosity to prevent spreading. This thixotropic behavior preserves the printed line geometry.[54,56] Without it, the paste may be conductive, but the printed pattern will be poor. Fig. 5 shows a representative example of high-resolution screen printing of graphene interconnects on flexible substrates. Fig. 5a first illustrates the screen-printing process using a flexible silicon stencil, where the graphene paste is transferred through the patterned opening under squeegee pressure. Fig. 5b and c show optical microscopy images of the printed graphene lines and source/drain electrodes, confirming that line widths down to 40 μm can be obtained with well-defined printed features. Fig. 5d further shows the test pattern used to evaluate the electrical properties of graphene lines with different printed widths and lengths. The SEM image in Fig. 5e reveals the

morphology of the annealed graphene film, where the flake network forms a continuous conducting pathway after post-treatment. The resistance data in Fig. 5f show that the resistance per unit length decreases as the printed line width increases, which is expected from the larger conducting cross-section. Finally, Fig. 5g demonstrates the mechanical reliability of the printed graphene lines under repeated bending, where the relative resistance remains stable over 1000 bending cycles at a 4 mm bending radius. Therefore, Fig. 5 supports the discussion that screen printing is suitable for relatively thick and mechanically reliable graphene interconnects, especially when low resistance and flexible-substrate compatibility are more important than ultrafine resolution.[57]

Post-processing is particularly important for screen-printed graphene because the printed film is thick and porous. Compression rolling or calendering after annealing can densify the film, improve flake overlapping and reduce inter-flake contact resistance. Conductivities upto 8.81×10^4 S/m have been reported for optimized screen-printed graphene films, which is among the higher values for printed carbon conductors.[54] The gain comes from network densification, not from changing the intrinsic graphene itself.

3.4 Gravure Printing

Gravure printing is more relevant when graphene interconnects are considered from a manufacturing viewpoint rather than only from a laboratory prototyping viewpoint. The main advantage of this technique is its direct compatibility with roll-to-roll (R2R) processing, where the patterned ink is transferred continuously from an engraved cylinder to a flexible substrate. The process involves three basic steps: filling of the engraved micro-cells with ink, removal of excess ink from the cylinder surface using a doctor blade, and transfer of the retained ink to the substrate through the nip pressure between the gravure roll and impression roller. Therefore, the final printed feature is not only determined by the ink formulation, but also by the cell geometry, doctoring condition and ink release from the engraved cavity.[8,29]

The ink rheology governs the transfer quality in gravure printing. Unlike screen printing, gravure requires relatively low-viscosity inks, typically in the range of 0.05–0.2 Pa·s, so that the ink can fill the engraved cells and detach cleanly during the nip-transfer process.[8] If the viscosity is too low, the ink can spread uncontrollably after transfer and result in edge blurring. If the viscosity is too high, the cell emptying becomes incomplete and the printed line becomes discontinuous. For graphene inks, ethyl cellulose (EC)-stabilized pristine graphene flakes in high-boiling solvents such as terpineol have been widely used because this combination provides sufficient dispersion stability, controlled drying and acceptable film formation. One important point to note is that the surface energy matching between the ink, engraved cell and substrate also controls the transfer efficiency. The interfacial energy is generally tuned close to the graphitic surface energy, around 40 mJ/m², to reduce the work required for ink detachment from the cell.[29,43]

The formation of a continuous graphene line in gravure printing is different from that in inkjet printing. In gravure, the printed line is built by the merging of many small ink volumes released from individual engraved cells. Therefore, the cell-spacing-to-cell-size ratio becomes a critical geometrical parameter. A small spacing-to-size ratio, around 0.1, helps neighboring droplets merge into a continuous wire without leaving gaps between the deposits. However, excessive spreading can also compromise the line resolution. This is the trade-off point in gravure printing — the ink must spread enough to form a continuous conductive pathway, but not so much that the printed line loses edge definition. Fig. 6 shows how gravure printing converts a low-viscosity graphene ink into continuous conductive patterns through cell filling, ink release and post-printing densification. Fig. 6a first illustrates the three basic steps of the gravure process: flooding of the engraved cells with graphene ink, removal of excess ink by doctor blading, and transfer of the retained ink to the substrate during printing. Fig. 6b shows the

printed graphene pattern, confirming that continuous lines can be formed when the ink release and cell geometry are properly controlled. The line-resistance data in Fig. 6c further show that the cavity size directly affects the electrical resistance of the printed features, because larger cavities can transfer a greater ink volume and form thicker conducting paths. Fig. 6d highlights the strong thickness contraction during annealing, which is caused by solvent removal and partial decomposition of the ethyl cellulose stabilizer. This shrinkage is useful to some extent because it densifies the graphene network and improves flake-to-flake contact. The AFM image in Fig. 6e shows that the final printed line is very thin compared with the substrate roughness, indicating why surface morphology and ink wetting are critical in gravure-printed graphene lines. Finally, Fig. 6f and g demonstrate printed crossbar and large-area patterns, showing the relevance of gravure printing for scalable and patterned graphene interconnect fabrication. Therefore, Fig. 6 supports the discussion that gravure printing is attractive for high-throughput graphene patterning, but its electrical performance depends strongly on cell design, ink transfer efficiency and annealing-induced network densification.[29]

The as-printed graphene films obtained by gravure are usually very thin, often in the range of 100–200 nm before annealing. During thermal treatment, partial decomposition and removal of the polymer stabilizer cause strong vertical shrinkage, and the final film thickness can reduce to nearly 15% of the original value, typically around 15–30 nm. This thickness reduction is not only a geometrical change. It also densifies the graphene network and improves inter-flake contact, which is important for lowering the sheet resistance. Optimized gravure-printed graphene lines have shown conductivities around 10^4 S/m and stable electrical continuity over hundreds of bending cycles. The conductivity is still far below metal interconnects, but the method offers a practical route for high-throughput graphene patterning on flexible substrates.[29]

3.5 Electrohydrodynamic Printing

Electrohydrodynamic (EHD) printing occupies a different space compared to inkjet, aerosol jet and screen printing. It is mainly useful when the required feature size approaches the fine-pitch region of ultra-thin chip integration and high-density signal routing. In conventional inkjet printing, the droplet size is strongly linked to the nozzle diameter. In EHD printing, the ink ejection is driven by an electric field rather than only by pressure or piezoelectric actuation. When a sufficiently high voltage is applied between the nozzle and substrate, the liquid meniscus deforms into a Taylor cone, and a very small jet or droplet is extracted from the cone apex. This allows the printed feature size to become much smaller than the nozzle diameter. This is the main reason EHD printing can reach sub-10 μm, and in some cases nearly 1 μm, pattern resolution.[3,15,41]

The ink requirement for EHD printing is also different from that of conventional direct writing. The ink must be sufficiently conductive or polarizable to respond to the electric field, but it should not become unstable during jet formation. Low-viscosity Newtonian inks, often below 500 mPa·s, are generally preferred because they allow stable cone-jet operation and controlled deposition. For FHE interconnects, this becomes important in two ways.

First, EHD printing can produce very narrow conductive lines for fine-pitch redistribution. Second, it can be used for vertical interconnect access formation, where small ink volumes must be deposited accurately into micro-via openings. This is particularly useful for Ag nanoparticle inks with particle sizes of 3–8 nm, which can fill small step heights more reliably than highly viscous extrusion pastes.[3,41]

For graphene-based patterns, the main advantage of EHD-related printing is the possibility of aggressive dimensional scaling. Recent EHD-assisted and maskless transfer-printing approaches have demonstrated graphene line widths around 3.2 μm with spacing close to 1 μm. This is a significant improvement over conventional inkjet-printed graphene, where the line width is usually limited to tens of micrometers. The high resolution is achieved by

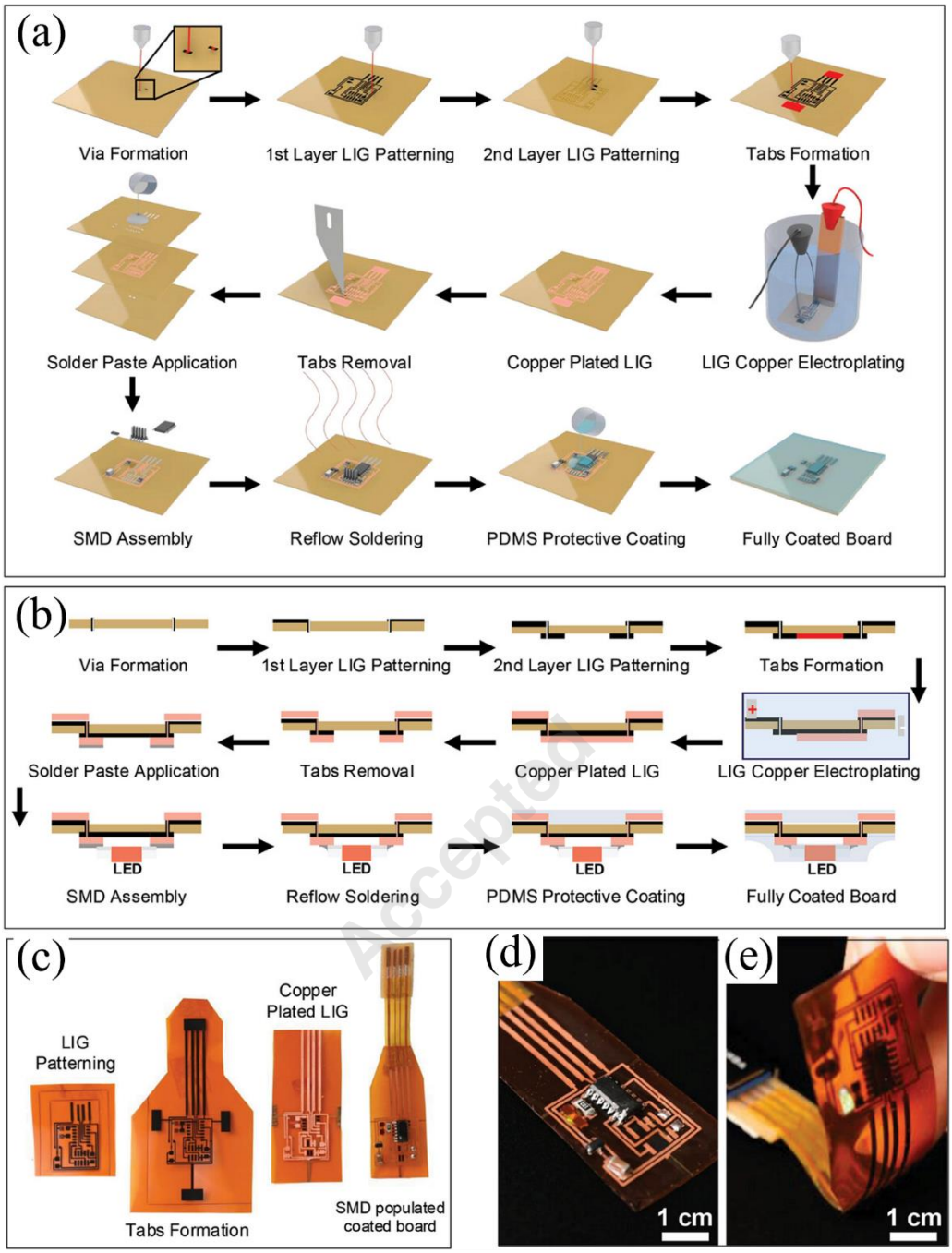

Fig. 7. Process flow of the E-LIG fabrication method for printed electronics. a) Schematic illustration of the full streamlined fabrication process including LIG patterning, from two sides followed by via and tab formation. After copper plating, the tabs are removed, solder paste is applied, and surface mount devices (SMDs) are assembled. b) Cross-sectional diagram illustrating the step-by-step development of the PCBs. c) Photographs showing the progression on the original polyamide substrate including the intermediate and final stages of the PCB fabrication process. d) Photograph of the fully assembled and functional double-sided flexible PCB with e) a LED on the bottom layer. Adapted with permission from [64].

controlling the wetting and dewetting of the graphene ink on smooth hydrophobic molds, such as Cytop-coated silicon. In this case, the mold does not only define the line width, but also improves the line edge roughness, which can be reduced to below 25 nm. This level of edge

control is important when printed graphene is used near chip pads or dense interconnect layouts.[41]

The electrical performance of EHD-templated graphene patterns is also promising. Sheet resistance values around 35 ± 6 ohm/sq have been reported for 10 µm graphene lines, while the patterns maintained stable performance under cyclic bending at about 1% tensile strain. It is important to note that this strain value is not a stretchable-electronics benchmark, but it is relevant for fine-pitch interconnects near rigid chip interfaces where the local strain must be minimized. Therefore, EHD printing should not be viewed as a high-throughput replacement for screen or gravure printing. It is better positioned as a high-resolution printing method for local interconnects, chip-to-flex interfaces, micro-vias and fine redistribution layers.

Its practical limitation is throughput and process complexity, but its strength is precision. This makes EHD printing an important tool for scaling graphene-based FHE toward higher circuit density.[41] The major printing techniques for graphene-based interconnect fabrication are compared in Table 2. In general, inkjet printing is suitable for digital prototyping and multilayer layouts, but its low film thickness per pass limits its use for low-resistance power lines. AJP offers better resolution and conformal printing capability, making it useful for fine-pitch die routing and non-planar surfaces. Screen printing is more suitable for thick, low-resistance interconnects and high-throughput fabrication, whereas gravure printing is attractive for large-area roll-to-roll manufacturing. EHD printing provides the highest patterning resolution and is therefore useful for micro-vias and ultra-thin chip integration, although its throughput remains limited. Therefore, the selection of printing techniques should be based on the required balance between resolution, film thickness, conductivity, throughput and substrate geometry.

Table 2. Printing technique comparison for graphene interconnects in terms of ink rheology, resolution, film thickness, conductivity, throughput and application suitability.

Technique	Viscosity Window	Resolution	Thickness per Pass	Reported Conductivity	Throughput	Best-fit Application	Ref
Inkjet Printing	1–30 mPa·s	20–50 µm	< 200 nm	3.91×10^4 S/m	Moderate (Digital)	Digital prototyping and complex multi-layered layouts	[13,17]
Aerosol Jet (AJP)	1–1000 mPa·s	5–20 µm	100–700 nm	$\sim5\times10^4$ S/m	Moderate (Digital)	Conformal printing on 3D/curved surfaces and fine-pitch die routing	[20,44,51]
Screen Printing	1–10 Pa·s	40–100 µm	5–25 µm	8.81×10^4 S/m	High (Roll-to-Roll)	Power buses, ground planes, and high-volume manufacturing	[55,57]
Gravure Printing	50–200 mPa·s	~30 µm	15–30 nm	$\sim1\times10^4$ S/m	Very High (up to 15 m/s)	Large-area, industrial-scale high-speed production	[32,44]
EHD Printing	≤ 500 mPa·s	1–10 µm	Nanoscale	35 ± 6 Ω/sq (Sheet Res.)	Low (High-res focus)	Micro-VIAs, ultra-thin chip integration, and nanoelectronics	[3,42]

Note: The values listed are representative ranges reported for graphene-based printed interconnects and may vary depending on ink formulation, substrate, post-treatment and printing parameters.

4. Via Formation and 3D Interconnects

4.1 Vertical Interconnect Challenges in Flexible Substrates

The progress from single-layer flexible circuits to complex multilayer FHE requires reliable vertical interconnect access structures. Without vias, flexible circuits remain mostly limited to planar routing, which increases

footprint and prevents compact integration of ultra-thin chips, sensors and antennas. In rigid microelectronics, through-silicon vias (TSVs) and electroplated copper structures are matured technologies. In flexible substrates, the same approach cannot be directly transferred because the substrates are soft, thermally limited and mechanically unstable under bending.[2,3,58]

The substrate is the first limitation. PI is widely used in flexible printed circuits because it has high thermal stability, with glass transition temperature above 400°C, and good chemical resistance.[1,59] But PI is relatively expensive and often needs laser drilling or aggressive patterning steps. PET and PEN are cheaper and transparent, but their thermal budgets are much lower, generally around 80–120°C for PET/PEN-type processing windows. This makes high-temperature sintering difficult. Paper and textile substrates introduce another issue: the porous network absorbs the ink and disturbs via filling unless a planarization layer is used. Therefore, the via process must be designed around the substrate, not only around the conductive ink.

Poor step coverage is the most common failure mode in printed vias.[1,4,59] In an electroplated Cu via, the metal can be grown thick and continuous along the sidewalls. In printed vias, the ink has to wet the sidewall, fill the via mouth and remain continuous after solvent evaporation. During drying, the film shrinks and stress concentrates near the via collar. This can produce cracks, delamination or discontinuity at the sharp edge of the hole. High aspect ratio vias are even more difficult because viscous inks may coat the upper wall without reaching the bottom. This gives an apparently filled via, but electrically the connection is unstable.[60]

4.2 Printing based via formation

Printing-based via formation usually starts with hole formation followed by conductive ink infiltration. CO_2 lasers at 10.6 μm are commonly used for PI because the polymer absorbs strongly at this wavelength. The drawback is that thermal ablation can leave carbonized residues and a heat-affected zone. Ultrashort pulsed (Picosecond and femtosecond) lasers reduce this problem by cold ablation, producing cleaner microvias with diameters upto 10 μm and sharper edges. [58,61] The laser step determines the via wall quality, which in turn determines the ink filling quality.

Once the through-hole is formed, ink infiltration is governed by wetting, viscosity and drying dynamics. The ink must flow into the via during deposition, but it should not slump or drain out before solidification. The non-Newtonian and Shear-thinning inks are useful because they have low viscosity under printing stress and regain viscosity after deposition.[2,62] Layer-by-layer inkjet filling can be used for prototyping, but the coffee-ring effect becomes severe inside the confined via geometry. Flakes can move toward the via edge and leave the center underfilled. This increases contact resistance and causes early failure under current stressing.

AJP is a stronger method for high-aspect-ratio via filling because the focused aerosol beam can deliver material into recessed or non-planar regions without direct nozzle contact. Phase-inversion graphene inks are particularly interesting in this context. By adding a low-volatility nonsolvent such as glycerol, the ink can change from a low-viscosity aerosol-compatible state to a gel-like deposited state after impact. This gelation process prevents the collapse during drying and allows 2.5D pillar structures with aspect ratios upto 10.[52] The important point is that the via is not filled only by volume deposition; it is stabilized by an ink rheology transition.

4.3 Graphene/metal hybrid Vias

Graphene-metal hybrid vias are used because pure graphene vias usually lack the raw conductivity required for dense power routing. In hybrid vias, Ag or Cu provides the main conductive path, while graphene acts as a crack-bridging and mechanically compliant

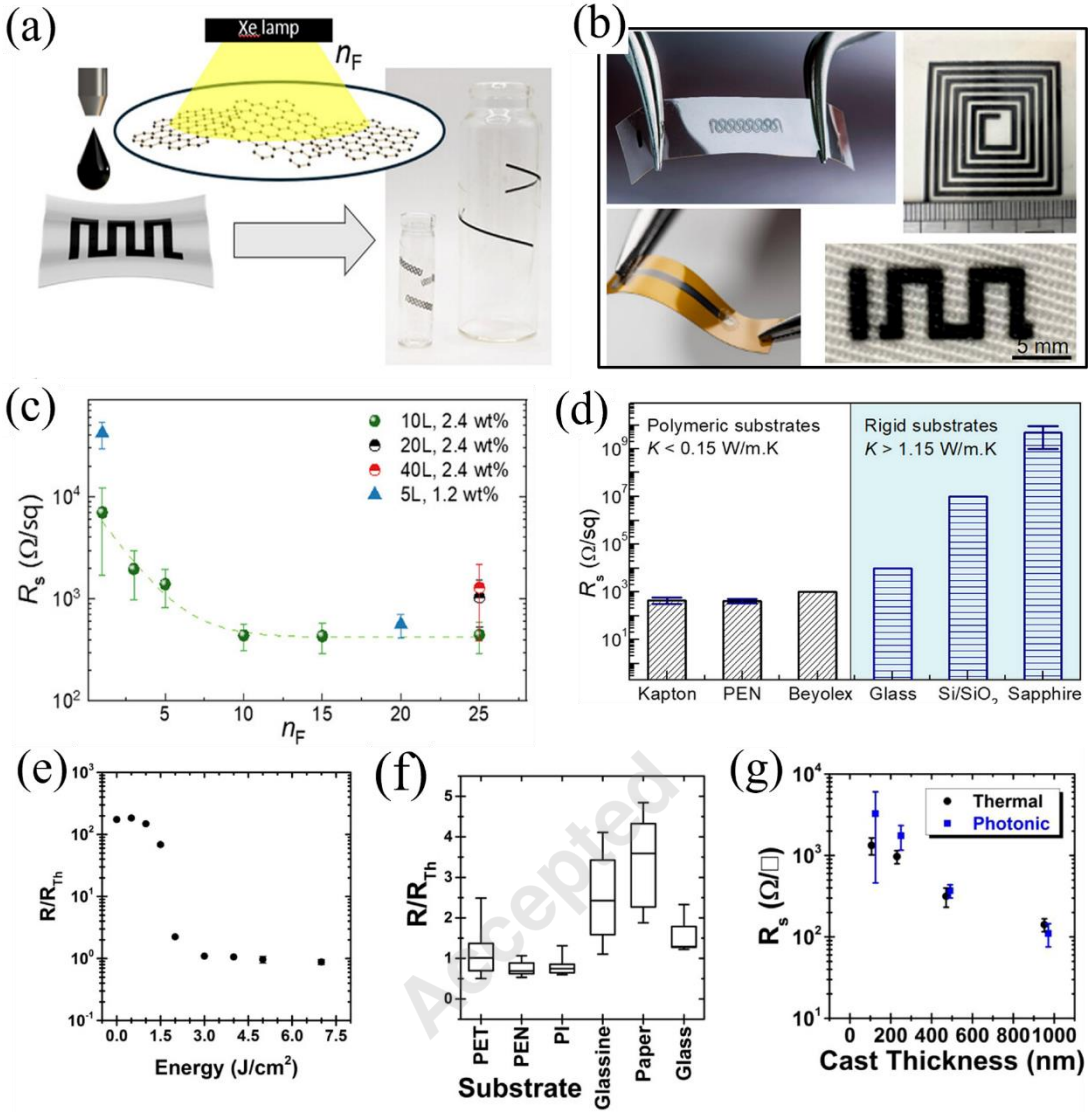

Fig. 8. Photonic annealing for conductivity enhancement of the printed interconnects. (a) Schematic diagram of the intense pulsed light (IPL) photonic annealing process being used on an iGr pattern to enable conductive films on a stretchable Beyolex substrate. b) Optical images of iGr prints on Beyolex (top left, print size 1×0.2 cm), PEN (top right), Kapton (bottom left, size 4×0.5 cm) and fabric (bottom right) c) Dependence of the sheet resistance of iGr samples on the number of printed layers, n_L (1.2 wt.% ink, Samba) post-processed with different numbers of IPL flashes $1 < n_F < 25$. (d) Sheet resistance, R_s of photonically annealed iGr samples (n_L = 10 printed layers, 2.4 wt.% ink, DMC, n_F=10) printed on polymeric substrates (thermal conductivity K<0.15 W m.K^{-1}) and on rigid substrates (K >1.15 W m.K^{-1}). Adapted with permission from [70]. Copyright © 1999-2026 John Wiley & Sons, Inc. Electrical characterization of photonically annealed graphene/nitrocellulose films. (e) Sheet resistance as a function of photonic annealing pulse energy on glass; each data point shows the average and standard deviation for three samples. (f) Normalized sheet resistance relative to thermal annealing for graphene/nitrocellulose films on various substrates. (g) Sheet resistance for graphene/nitrocellulose films as a function of thickness following thermal and photonic annealing on glass. The reported thickness corresponds to the thickness prior to annealing (photonic annealing leads to thicker films with the same amount of material due to the resulting porous microstructure). Adapted with permission from [72]. Copyright © 2017 American Chemical Society.

interface.[63] During bending or thermal cycling, metallic nanoparticle films can develop microcracks. Graphene flakes can bridge these cracks and maintain percolation across damaged

regions. Hybrid graphene/Ag structures can therefore give much lower resistivity than pure graphene while maintaining better fatigue resistance than metal-only vias.

Laser-induced graphene (LIG) offers a different route for vertical interconnects.[64,65] Instead of printing an external ink on a PI substrate, a CO_2 laser irradiation can convert the sp^3 carbon in PI into porous sp^2-rich graphene under ambient conditions. In a double-sided flexible circuit, the laser can ablate a hole and carbonize the rim of the via at the same time, forming a conductive ring between the top and bottom layers. Bare LIG is relatively resistive, around 50 ohm/sq, but it works well as a porous seed layer for copper plating. When Cu is deposited into the LIG framework, the resulting Cu-LIG composite can approach 1.67×10^6 S/m conductivity.[64,66] This is not purely a graphene via anymore. It is a graphene-assisted metal via. Fig. 7 shows a representative route for forming double-sided flexible printed circuits using laser-induced graphene followed by metallization. Fig. 7a first presents the overall E-LIG fabrication sequence, where graphene patterns are generated on both sides of the polyimide substrate, followed by via and tab formation, copper plating, tab removal, solder paste deposition and SMD assembly. This process flow is important because it shows that laser-written graphene can act not only as a printed conductor, but also as a seed layer for subsequent metal reinforcement. Fig. 7b gives the corresponding cross-sectional view of the structure at different fabrication stages, clarifying how the top and bottom conductive layers are connected through the via region. The photographic images in Fig. 7c show the practical progression of the flexible PCB from the original polyimide substrate to the intermediate and final fabrication stages, which confirms the process compatibility with large-area flexible substrates. Finally, Fig. 7d and e show the assembled double-sided flexible PCB and the operating LED on the bottom layer, demonstrating that the formed interconnects and vias can support functional device integration. Therefore, Fig. 7 supports the discussion that graphene-based via structures can be used as part of a hybrid interconnection strategy, especially when combined with metal plating to reduce resistance and improve circuit-level reliability.[64,67]

Other 3D graphene structures, including graphene foams and laser-sintered porous carbon architectures, are also being explored for vertical interconnects. Their high porosity and mechanical compliance can help absorb bending-induced strain in system-in-foil architectures.[65,68] However, these structures are still far from standardized interconnect technologies. The immediate practical route is more likely to be hybrid via structures, where graphene contributes mechanical stability, oxidation resistance or crack bridging, while metal provides the main current path.

Though the early printed vias reportedly suffered from high contact resistances, recent progress has shown noticeable improvements. For example, the optimized EHD and extrusion based silver vias have achieved resistance values as low as <2 ohms, for the step heights of 4 μm.[3] In the case of AJP graphene interconnects, the power dissipation is reportedly limited by the thermal resistance of polymer substrate, and therefore the thermal-aware design is highly important in 3D integration. [69]

5. Conductivity enhancement, mechanical reliability and integration

5.1 Conductivity enhancement

The electrical performance of printed graphene interconnects is limited in the as-deposited state. Freshly printed films contain solvent residues, polymer stabilizers, voids and weak flake-to-flake contacts. Therefore, post-processing is essential to convert a printed carbon coating into an interconnect. The main aim is to remove insulating residues, increase packing density and reduce the inter-flake tunneling barrier.[28,70]

5.1.1 Thermal Annealing

Thermal annealing is the conventional method for conductivity improvement. The

useful temperature range is defined by the substrate thermal budget.

PET is generally limited to less than 150°C, PEN to less than 200°C, while PI can tolerate 350–400°C. Paper substrates are usually kept close to 100°C to avoid charring.[2,28,54,70] This means the same graphene ink can give different conductivities on different substrates, simply because the binder cannot be removed equally.

The improvement during annealing comes mainly from binder decomposition, solvent removal and flake coalescence. EC, PVP and similar stabilizers surround the graphene flakes and create a dielectric barrier between them. When the film is heated, these organic components decompose or volatilize, and the flakes come into closer contact. In some cases, aromatic carbon residues can assist π-π interaction between flakes and act as a weak conductive bridge. Thermal annealing can improve conductivity by 10–100 times, often pushing the film above 10^4 S/m.[13,24,49] While the incomplete annealing leaves residues, too aggressive annealing damages the substrate.

5.1.2 Photonic and Laser Processing

Photonic annealing is useful when the substrate cannot withstand long thermal exposure. For example, intense light sources such as xenon flash lamps to heat the printed graphene film within milliseconds. Graphene absorbs light strongly, so the printed trace can reach temperatures above 250°C while the bulk polymer substrate remains comparatively cool.[12,70,71] This selective photothermal heating is especially useful for PET and other low-temperature foils. The risk is non-uniform heating if the film thickness or optical absorption is not uniform. Fig. 8 shows the role of photonic annealing in improving the conductivity of printed graphene interconnects on both flexible and rigid substrates. Fig. 8a first illustrates the intense pulsed light (IPL) annealing process, where short high-energy light pulses are used to locally heat the printed graphene pattern without exposing the whole substrate to a high thermal budget. This is particularly important for polymer substrates, where conventional thermal annealing can cause deformation or thermal damage. Fig. 8b shows optical images of inkjet-printed graphene patterns on different substrates such as Beyolex, PEN, Kapton and fabric, confirming that the same post-processing route can be applied across mechanically different flexible platforms. The sheet-resistance comparison in Fig. 8c shows that the substrate thermal conductivity strongly affects the photonic annealing response, since low-thermal-conductivity polymer substrates retain heat differently from rigid substrates. Fig. 8e further shows the effect of pulse energy on sheet resistance, indicating that the annealing energy must be optimized to remove insulating residues and improve graphene network connectivity without damaging the film. Fig. 8f compares the normalized sheet resistance after photonic and thermal annealing on different substrates, showing the advantage of photonic processing for temperature-sensitive substrates. Finally, Fig. 8g shows the thickness-dependent sheet resistance of graphene/nitrocellulose films, confirming that both film thickness and annealing method control the final electrical performance. Therefore, Fig. 8 supports the point that conductivity enhancement in printed graphene interconnects is not governed only by the graphene source, but also by the post-processing route, substrate thermal properties and printed-film thickness.[70,72]

Laser processing provides even more localized treatment. By controlling the laser fluence, the printed trace can be annealed, sintered or partially graphitized without heating the whole substrate.[6,66] In LIG processing, the same principle is extended to directly convert PI into porous graphene. Photonic and laser treatments are attractive for roll-to-roll manufacturing because they are fast and compatible with ambient processing. However, they require careful energy control. Too little energy leaves the binder behind, while too much energy burns the film or deforms the substrate.

5.1.3 Mechanical and Chemical Treatments

Mechanical compression/calendaring are useful in improving the electrical conductivity of printed FHE interconnects, by addressing the inherent porosity of the printed graphene flakes. The printed patterns/film are densified by applying pressure through a roller, which eventually increases the flake to flake overlapping and decreases the inter-flake distance of non-contacting flakes to within the tunneling regime (<3 nm).[54,73] This physical lamination yields a conductivity improvement of 2–5x, and in binder-free systems, the enhancement can be upto 50x. The advantage of calendering is that it does not depend strongly on substrate temperature. The limitation is that excessive pressure can damage soft substrates or crack brittle underlying layers.

Chemical doping is another route to reduce resistance. Acids such as HNO_3 or dopants such as $AuCl_3$ can increase hole concentration in graphene and lower sheet resistance.[6,54] The improvement can be large, but stability is the main problem. Many dopants are sensitive to ambient moisture, oxygen or heat, and the conductivity can degrade over weeks or months. Therefore, chemical doping is useful for demonstrating high conductivity, but it is not automatically a reliable manufacturing solution. Combined treatments such as calendering followed by thermal or photonic annealing are often more realistic because they improve both network density and residue removal.

5.2 Mechanical Reliability

5.2.1 Bending and Folding

The mechanical robustness of the printed interconnects is characterized by the relative change in resistance ($\Delta R/R_0$) as the function of bending radius (r_c) of the substrate. Unlike bulk metals interconnects and transparent oxides, graphene-based printed interconnects maintain electrical robustness at extreme radii (<2 mm).[13,49] The conventional metal-based interconnects exhibit failure or unpredictable resistance changes after 750-1000 bending cycles, due to irreversible crack formation. However, graphene-based interconnects can withstand 1500-10,000 cycles, with resistance variation less than 5%.[24,54,66] This performance flexibility is attributed to the percolated graphene network. In other words, when a substrate with graphene interconnect undergoes deformation or bending, the graphene flakes slide over each other to maintain the electrical contact within. Furthermore, establishment of new tunneling junctions under deformation helps to retain the original electrical conductivity.

5.2.2 Stretching and Environmental Stability

The stretchable interconnects need to overcome the mechanical mismatch between the printed interconnects and the elastic substrates. The conventional metal interconnects fail when stretched, due to the channel cracks perpendicular to the strain.[6,74] In the case of graphene, the crack paths can be deflected by the percolated graphene network, and it can undergo stable, serrated failure when reinforced with specific binders. The printed interconnects can withstand strain over 100% when the structural strategies such as serpentine geometries, kirigami patterns and/or pre-strained (PDMS, TPU) are used.[6,75] These strategies help to decouple the global elongation of the substrate from the local material stress.

Environmental stability of the printed interconnects is essential to maintain reliability, since humidity and temperature cycling can change the resistance by swelling the binder, oxidizing metal fillers or weakening adhesion at the substrate interface. The choice of binder can determine the stability of the interconnects, for e.g., nitrocellulose binder has shown good resistance stability under 85°C/85% RH damp heat testing, whereas ethyl cellulose based interconnects tend to degrade upto 50%.[2] Encapsulation of printed interconnects with stable polymer films, such as PI or silicone can protect them from moisture and oxygen attack, which in turn can expand their lifespan without appreciable degradation.[76] The mechanical advantage of graphene-based interconnects compared with conventional metal nanoparticle interconnects is summarized in Fig. 9. In conventional Ag nanoparticle interconnects, repeated deformation can induce crack formation, particle separation and void growth, leading to rapid resistance increase. In contrast, printed graphene networks can accommodate deformation through flake sliding, overlap reconfiguration and crack bridging, thereby maintaining the conductive percolation pathway.

In graphene/Ag hybrid interconnects, the graphene scaffold further bridges separated Ag nanoparticles and suppresses crack opening, providing a balance between enhanced conductivity and improved cyclic stability.

5.3 Integration into Flexible Hybrid Electronics

budget of many polymer foils, while Sn-Bi solder and anisotropic conductive films (ACF) can operate around 100–150°C.[1,2] Graphene can also act as a solder-compatible barrier when printed over Ag traces. During soldering, Ag can dissolve or react with flux, which weakens the contact.[77] A graphene overlayer can reduce

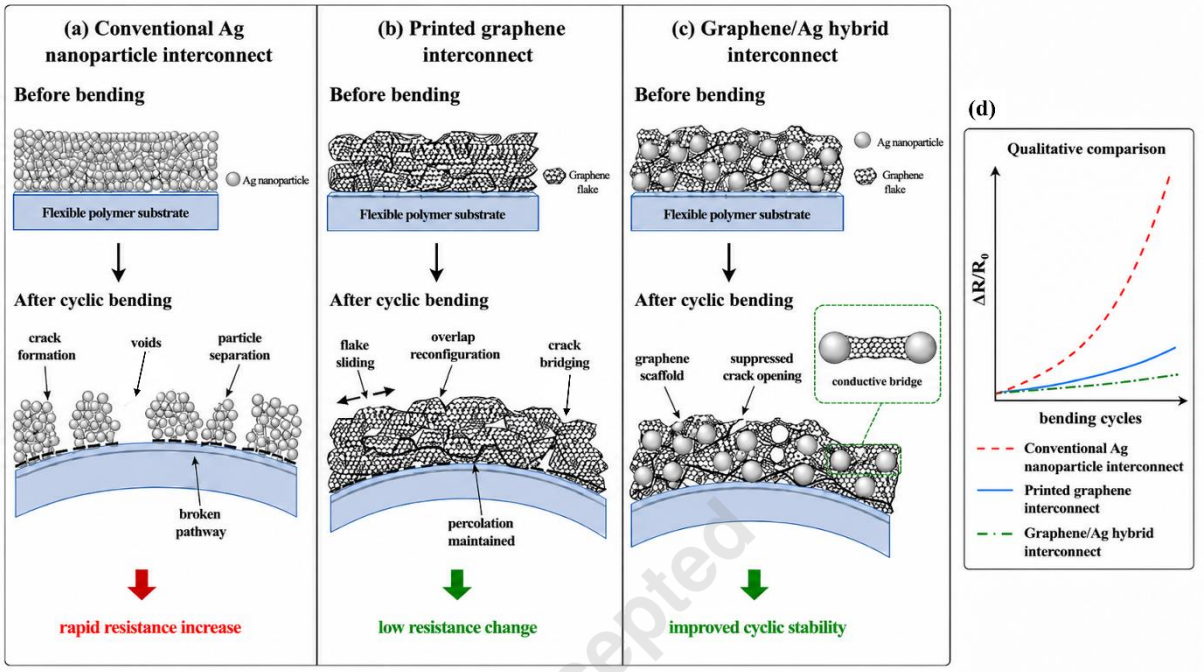

Fig. 9. Schematic comparison of cyclic bending reliability in conventional Ag nanoparticle, printed graphene, and graphene/Ag hybrid interconnects. (a) Conventional Ag nanoparticle interconnects can undergo crack formation, void generation, particle separation, and eventual conductive-pathway failure under repeated bending, resulting in a rapid increase in resistance. (b) Printed graphene interconnects maintain electrical continuity more effectively because graphene flakes can slide, overlap, bridge local cracks, and preserve percolation pathways during deformation. (c) In graphene/Ag hybrid interconnects, graphene flakes act as a mechanical scaffold and conductive bridge between Ag nanoparticles, suppressing crack opening and improving cyclic stability. (d) The qualitative plot summarizes the expected change in normalized resistance $(\Delta R/R_0)$with bending cycles for the three interconnect types.

The use of printed graphene in FHE depends not only on the printed line itself, but also on how it connects with rigid silicon chips, metal pads, dielectrics and encapsulation layers. This interface between soft printed conductors and rigid components is often the weak point in the system. A graphene interconnect may be mechanically robust, but the device can still fail at the chip pad, solder joint or via contact.

5.3.1 Interfacing and Redistribution Layers

Interfacing rigid IC pads with printed graphene requires low-temperature bonding. Conventional Sn-Pb solders exceed the thermal

this degradation and maintain a stable interface. This is a useful role because graphene is not only acting as the conductor, but also as a protective interfacial layer.

Printed graphene can also function as a redistribution layer (RDL) or fan-out interconnect. Ultra-thin silicon chips can have pad pitches below 50 μm, while large-area printed circuits usually have much coarser resolution.[2] The RDL bridges this geometry mismatch by redistributing fine chip contacts to wider printed traces. This is an important application area for AJP and inkjet printing

because both can create localized patterns without full-area lithography.

5.3.2 Multi-layer Circuits and Dielectrics

Multilayer FHE circuits require printed dielectrics and reliable vias. PVP, SU-8 and PI are commonly used as insulating layers, while Ag, graphene or hybrid inks form the interconnect levels.[1,3,66] AJP is particularly useful for sequential deposition of ground planes, dielectric layers and sensing/interconnect layers. However, registration accuracy remains a serious issue. If the alignment error is on the order of tens of micrometers, the via may miss the pad or the printed conductor may short with the adjacent layer. Therefore, multilayer printing is not only a material problem. It is a registration and process-control problem.

Graphene-based FHE demonstrations are most convincing when the material advantage is connected to the device requirement. Wearable electrophysiological sensors use graphene because of its flexibility, large surface area and reasonable skin compatibility.[24,77] Biochemical sensing platforms use graphene because the surface is sensitive to ionic and molecular interactions. Flexible RFID antennas and paper-based RF tags use graphene because bendability and lightweight form factor are more important than absolute metal-like conductivity.[54,73] The field should avoid presenting graphene as a universal replacement for Ag or Cu. Its stronger position is in mechanically demanding, chemically sensitive and low-temperature printable systems where metals alone face reliability limitations.

6. Summary and outlook

The central challenge of printed graphene interconnects in FHE is not one of intrinsic material capability — it is the persistent gap between what a single graphene flake can do and what a disordered printed network actually delivers. This review has examined that gap from every practical angle. On the ink side, EEG-derived flakes with large lateral dimensions and low defect density offer the highest printed conductivity, reaching upto ~10^5 S/m, but scalability and electrolyte removal remain unresolved. LPE graphene is the more widely deployed source, which reliably produces interconnects in the 1–5×10^4 S/m range after annealing, which is sufficient for signal routing but not for power delivery. rGO closes the cost barrier, at the expense of a permanently disrupted sp^2 network that no amount of reduction fully restores. Across all three, the inter-flake junction resistance is the bottleneck, and closing it requires not just better flakes but better network architecture. Hybrid graphene/Ag inks represent the most practical near-term solution: Ag nanoparticles fill the inter-flake gaps and lower percolation resistance, while the graphene scaffold bridges microcracks and suppresses electromigration. The conductivity-flexibility trade-off in these systems is real, but it is manageable when the graphene-to-metal ratio is matched to the application — leaning graphene-rich for mechanically demanding wearable routes, and metal-rich for static redistribution layers.

On the printing side, no single method dominates. Inkjet printing is well-suited to signal routing at 20–50 µm resolution, but coffee-ring suppression through Marangoni flow engineering and substrate temperature control remains essential for achieving uniform film coverage. Aerosol jet printing is the method of choice for fine-pitch chip interconnection and via filling, enabled by its wide viscosity window and standoff-distance advantage, though overspray management and registration accuracy over large areas are still limiting factors. Screen printing remains the most productive route for power bus fabrication, delivering thick graphene films with conductivities approaching ~10^4–10^5 S/m range after calendaring, in which the gains originate from network densification, not from the graphene itself changing. Via formation, the most underexplored area in the graphene interconnect literature, has been treated with particular attention here. Hybrid graphene-assisted

metallization, where graphene or LIG provides a mechanically compliant seed or crack-bridging interface and copper provides the primary conductive path — represents the most promising direction for achieving practically viable vertical interconnects in multilayer FHE stacks. Pure graphene vias remain too resistive for current-dense applications. Mechanically, printed graphene interconnects maintain $\Delta R/R_0$ below 5% over 1,500–10,000 bending cycles depending on ink formulation and structural design, substantially outperforming sintered metal NP films, whose resistance rises sharply and often irreversibly after fewer than 1,000 cycles. The mechanism is not crack resistance — it is percolation reconfiguration: flake sliding, new junction formation and distributed current rerouting. This is the genuine materials advantage of graphene over metallic nanoparticle systems in mechanically dynamic FHE.

Graphene-based printed interconnects are not yet replacing silver nanoparticle inks at scale. The conductivity gap remains real, the processing infrastructure is less mature and the reliability database is thinner. Their stronger position, for now, is in mechanically demanding, thermally constrained and chemically sensitive applications where sintered metal films have already been shown to fail.

Several open problems define the direction of this field going forward. The most fundamental is the junction resistance problem. Inter-flake junctions remain the rate-limiting step in printed graphene conductivity, and while thermal annealing, photonic sintering and calendering each address it partially, none provides a manufacturing-compatible, substrate-agnostic solution. The emerging idea of chemical junction welding using π-conjugated bridging molecules or conformal metal coating at flake edges to create covalent or near-ohmic flake contacts has shown promise at the laboratory scale, but translation to roll-to-roll compatible processes is not established. MXene/graphene co-deposition is another direction worth watching: MXene's metallic conductivity and 2D morphology make it a natural junction-filling candidate within a graphene percolation network, and early results suggest the combination can outperform either component alone. More importantly, the second open problem is one that the field rarely acknowledges: there is no agreed benchmark for printed via resistance. Without a standardized test structure, such as specifying aspect ratio, substrate, anneal condition and measurement protocol, comparisons across literature are nearly impossible, and progress on via performance cannot be tracked reliably. This is a field-level gap that slows development more than any specific materials limitation.

Self-healing and damage-tolerant design represent a near-term opportunity that remains largely unexplored for printed interconnects. Graphene percolation networks reconfigure passively under deformation, but active recovery through encapsulants that refluidize at body temperature or through microcrack-triggered conductive healing agents — has not been demonstrated in a printed FHE context. The materials building blocks for this already exist in soft robotics and self-healing polymer research; the translation to printed interconnect stacks is a realistic short-term goal. Finally, the jump from laboratory-scale printing to roll-to-roll manufacturing remains the real commercialization barrier, and it is predominantly a process engineering problem rather than a materials one. Registration accuracy across large substrate areas, ink stability over multi-hour print runs, drying uniformity in high-throughput web processes and quality control for sub-50 μm features at roll speeds — these are the problems that will determine whether printed graphene interconnects move from demonstrations to deployed FHE products. They deserve considerably more research attention than the field currently directs toward them.

ABBREVIATIONS

Ag Silver
Cu copper
ACF Anisotropic Conductive Film
AFM Atomic Force Microscopy
AJP Aerosol Jet Printing
DLS Dynamic Light Scattering
DMC Dimethyl Carbonate
DMF Dimethylformamide
DOD Drop-On-Demand
EC Ethyl Cellulose
ECE Electrochemical Exfoliation
ECHA European Chemicals Agency
EDX Energy-Dispersive X-ray
EEG Electrochemically Exfoliated Graphene
EGT Electrochemical Gated Transistor
EHD Electrohydrodynamic
FHE Flexible Hybrid Electronics
FR Focusing Ratio
GO Graphene Oxide
HMDS Hexamethyldisilazane
IC Integrated Circuit
iGr Inkjet-printed Graphene
IPL Intense Pulsed Light
IPA Isopropyl Alcohol
LED Light-Emitting Diode
LIG Laser-Induced Graphene
LPE Liquid Phase Exfoliation
NC Nitrocellulose
NMP N-Methyl-2-Pyrrolidone
NP Nanoparticle
OM Optical Microscopy
PCB Printed Circuit Board
PDMS Polydimethylsiloxane
PEN Polyethylene Naphthalate
PET Polyethylene Terephthalate
PI Polyimide
PVP Polyvinylpyrrolidone
RDL Redistribution Layer
RF Radio Frequency
RFID Radio Frequency Identification
rGO Reduced Graphene Oxide
RH Relative Humidity
R2R Roll-to-Roll
SDS Sodium Dodecyl Sulfate
SEM Scanning Electron Microscopy
SMD Surface Mount Device
TLM Transfer Length Method
TPU Thermoplastic Polyurethane
TSV Through-Silicon Via

supplement 가 없는 논문은 아래 4 줄은 삭제 부탁 드립니다.

SUPPLEMENTARY INFORMATION

The online version contains supplementary material available at https://

ACKNOWLEDGEMENTS

하단의 3 가지 항목 삭제는 불가하며, 해당 사항이 없는 경우 기본 문구라도 적어주시기 바랍니다.

Author Contributions

G.B. conceived the review scope, conducted the literature survey, designed the manuscript structure, and drafted the manuscript. G.B. prepared all figures and tables. S.H. supervised the work, provided critical feedback on the manuscript, and revised the final version. All authors read and approved the final manuscript.

Funding

This research was partially supported by the XXX Grant Number XXX. (Times New Roman 10pt.)

해당 사항 없는 경우 기본 문구
Not applicable.

Declarations of Competing Interests

The authors declare that they have no competing interests.

AUTHORS

리뷰 논문만 AUTHORS 를 넣습니다.
하단 내용을 영문으로 작성해 주세요.

홍길동
2005~2009년: 서울대학교 XX학부 학사
2009~2007년: 서울대학교 XX학부 석사
[관심분야] 유연전자, 나노소재, 디스플레이, 발광체

박길동
2005~2009년: 서울대학교 XX학부 학사
2009~2007년: 서울대학교 XX학부 석사
[관심분야] 유연전자, 나노소재, 디스플레이, 발광체

REFERENCES

스타일별 예시를 적어두었고, [1], [2], [3]으로 나열해서 적어주시기 바랍니다.

(1) Khan, Y.; Thielens, A.; Muin, S.; Ting, J.; Baumbauer, C.; Arias, A. C. A New Frontier of Printed Electronics: Flexible Hybrid Electronics. Advanced Materials 2020, 32 (15), 1905279.
(2) Dahiya, A. S.; Christou, A.; Ma, S.; Dahiya, R. Printed Interconnects for Heterogeneous Systems Integration on Flexible Substrates. Adv Materials Technologies 2025, 10 (6), 2401213.
(3) Ma, S.; Dahiya, A. S.; Christou, A.; Zumeit, A.; Dahiya, R. High-Resolution Printing-Based Vertical Interconnects for Flexible Hybrid Electronics. Adv Materials Technologies 2024, 9 (17), 2400130.
(4) Zhao, Z.; Fu, H.; Tang, R.; Zhang, B.; Chen, Y.; Jiang, J. Failure Mechanisms in Flexible Electronics. International Journal of Smart and Nano Materials 2023, 14 (4), 510–565.
(5) Park, S.; Kim, H.; Kim, J.-H.; Yeo, W.-H. Advanced Nanomaterials, Printing Processes, and Applications for Flexible Hybrid Electronics. Materials 2020, 13 (16), 3587.
(6) Li, Y.; Veronica, A.; Ma, J.; Nyein, H. Y. Y. Materials, Structure, and Interface of Stretchable Interconnects for Wearable Bioelectronics. Advanced Materials 2025, 37 (23), 2408456.
(7) Kamyshny, A.; Magdassi, S. Conductive Nanomaterials for 2D and 3D Printed Flexible Electronics. Chem. Soc. Rev. 2019, 48 (6), 1712–1740.
(8) Htwe, Y. Z. N.; Mariatti, M. Printed Graphene and Hybrid Conductive Inks for Flexible, Stretchable, and Wearable Electronics: Progress, Opportunities, and Challenges. Journal of Science: Advanced Materials and Devices 2022, 7 (2), 100435.
(9) Jabari, E.; Ahmed, F.; Liravi, F.; Secor, E. B.; Lin, L.; Toyserkani, E. 2D Printing of Graphene: A Review. 2D Mater. 2019, 6 (4), 042004.
(10) Geim, A. K.; Novoselov, K. S. The Rise of Graphene. Nature Mater 2007, 6 (3), 183–191.
(11) Torrisi, F.; Carey, T. Graphene, Related Two-Dimensional Crystals and Hybrid Systems for Printed and Wearable Electronics. Nano Today 2018, 23, 73–96.
(12) Van Hazendonk, L. S.; Pinto, A. M.; Arapov, K.; Pillai, N.; Beurskens, M. R. C.; Teunissen, J.-P.; Sneck, A.; Smolander, M.; Rentrop, C. H. A.; Bouten, P. C. P.; Friedrich, H. Printed Stretchable Graphene Conductors for Wearable Technology. Chem. Mater. 2022, 34 (17), 8031–8042.
(13) Secor, E. B.; Prabhumirashi, P. L.; Puntambekar, K.; Geier, M. L.; Hersam, M. C. Inkjet Printing of High Conductivity, Flexible Graphene Patterns. J. Phys. Chem. Lett. 2013, 4 (8), 1347–1351.
(14) Karagiannidis, P. G.; Hodge, S. A.; Lombardi, L.; Tomarchio, F.; Decorde, N.; Milana, S.; Goykhman, I.; Su, Y.; Mesite, S. V.; Johnstone, D. N.; Leary, R. K.; Midgley, P. A.; Pugno, N. M.; Torrisi, F.; Ferrari, A. C. Microfluidization of Graphite and Formulation of Graphene-Based Conductive Inks. ACS Nano 2017, 11 (3), 2742–2755.
(15) Kralj, M.; Krivačić, S.; Ivanišević, I.; Zubak, M.; Supina, A.; Marciuš, M.; Halasz, I.; Kassal, P. Conductive Inks Based on Melamine Intercalated Graphene Nanosheets for Inkjet Printed Flexible Electronics. Nanomaterials 2022, 12 (17), 2936.
(16) Tomotoshi, D.; Kawasaki, H. Surface and Interface Designs in Copper-Based Conductive Inks for Printed/Flexible Electronics. Nanomaterials 2020, 10 (9), 1689.
(17) Parvez, K.; Worsley, R.; Alieva, A.; Felten, A.; Casiraghi, C. Water-Based and Inkjet Printable Inks Made by Electrochemically Exfoliated Graphene. Carbon 2019, 149, 213–221.
(18) Al Shboul, A.; Ketabi, M.; Skaf, D.; Nyayachavadi, A.; Lai Fak Yu, T.; Rautureau, T.; Rondeau-Gagné, S.; Izquierdo, R. Graphene Inks Printed by Aerosol Jet for Sensing Applications: The Role of Dispersant on the Inks' Formulation and Performance. Sensors 2023, 23 (16), 7151.
(19) Pei, S.; Cheng, H.-M. The Reduction of Graphene Oxide. Carbon 2012, 50 (9), 3210–3228.
(20) White, F.; Rektor, A.; Kouchi, F. R.; Varghese, T. V.; Pratap, A.; Burgoyne, H.; Chinnathambi, K.; Eixenberger, J.; Efaw, C.; Estes, L.; Murray, T.; Arumugam, P. U.; Subbaraman, H.; Estrada, D. Aerosol Jet Printing of Multilayered Graphene for Capacitive Touch Sensing and Joule Heating Applications. Advanced Sensor Research 2026, 5 (3), e00129.
(21) Safitri, R. N.; Suriani, A. B.; Htwe, Y. Z. N.; Muqoyyanah; Dwandaru, W. S. B.; Kumar, V. V.; Ali, K.; Othman, M. H. D.; Alluqmani, S. M.; Azlan, M. N.; Mamat, M. H. Recent

Development of Electrochemically Exfoliated Graphene and Its Hybrid Conductive Inks for Printed Electronics Applications. Synthetic Metals 2024, 308, 117707.

(22) Lim, H.; Kim, H. S.; Qazi, R.; Kwon, Y.; Jeong, J.; Yeo, W. Advanced Soft Materials, Sensor Integrations, and Applications of Wearable Flexible Hybrid Electronics in Healthcare, Energy, and Environment. Advanced Materials 2020, 32 (15), 1901924.

(23) Song, P.; Wang, G.; Zhang, Y. Preparation and Performance of Graphene/Carbon Black Silicone Rubber Composites Used for Highly Sensitive and Flexible Strain Sensors. Sensors and Actuators A: Physical 2021, 323, 112659.

(24) Kim, D. S.; Jeong, J.-M.; Park, H. J.; Kim, Y. K.; Lee, K. G.; Choi, B. G. Highly Concentrated, Conductive, Defect-Free Graphene Ink for Screen-Printed Sensor Application. Nano-Micro Lett. 2021, 13 (1), 87.

(25) Rijo, P. C.; Tocci, I.; Galindo-Rosales, F. J. Eco-Friendly Alternatives to Toluene-Based 2D Inks for Inkjet and Electrohydrodynamic Jet Printing Processes: A Rheological Study. Micromachines 2025, 16 (2), 130.

(26) Fernandes, J.; Nemala, S. S.; De Bellis, G.; Capasso, A. Green Solvents for the Liquid Phase Exfoliation Production of Graphene: The Promising Case of Cyrene. Front. Chem. 2022, 10, 878799.

(27) Torrisi, F.; Hasan, T.; Wu, W.; Sun, Z.; Lombardo, A.; Kulmala, T. S.; Hsieh, G.-W.; Jung, S.; Bonaccorso, F.; Paul, P. J.; Chu, D.; Ferrari, A. C. Inkjet-Printed Graphene Electronics. ACS Nano 2012, 6 (4), 2992–3006.

(28) Secor, E. B.; Ahn, B. Y.; Gao, T. Z.; Lewis, J. A.; Hersam, M. C. Rapid and Versatile Photonic Annealing of Graphene Inks for Flexible Printed Electronics. Advanced Materials 2015, 27 (42), 6683–6688.

(29) Secor, E. B.; Lim, S.; Zhang, H.; Frisbie, C. D.; Francis, L. F.; Hersam, M. C. Gravure Printing of Graphene for Large-area Flexible Electronics. Advanced Materials 2014, 26 (26), 4533–4538.

(30) Khan, J.; Mariatti, M. Effect of Natural Surfactant on the Performance of Reduced Graphene Oxide Conductive Ink. Journal of Cleaner Production 2022, 376, 134254.

(31) Sim, H. J.; Li, Z.; Xiao, P.; Lu, H. The Influence of Lateral Size and Oxidation of Graphene Oxide on Its Chemical Reduction and Electrical Conductivity of Reduced Graphene Oxide. Molecules 2022, 27 (22), 7840.

(32) Hernandez, Y.; Nicolosi, V.; Lotya, M.; Blighe, F. M.; Sun, Z.; De, S.; McGovern, I. T.; Holland, B.; Byrne, M.; Gun'Ko, Y. K.; Boland, J. J.; Niraj, P.; Duesberg, G.; Krishnamurthy, S.; Goodhue, R.; Hutchison, J.; Scardaci, V.; Ferrari, A. C.; Coleman, J. N. High-Yield Production of Graphene by Liquid-Phase Exfoliation of Graphite. Nature Nanotech 2008, 3 (9), 563–568.

(33) Secor, E. B.; Gao, T. Z.; Islam, A. E.; Rao, R.; Wallace, S. G.; Zhu, J.; Putz, K. W.; Maruyama, B.; Hersam, M. C. Enhanced Conductivity, Adhesion, and Environmental Stability of Printed Graphene Inks with Nitrocellulose. Chem. Mater. 2017, 29 (5), 2332–2340.

(34) Cai, R.; Liang, C.; Duan, Y.; Zhao, Z.; Zhang, X.; He, P.; Yang, J.; Lai, W.; Wei, J.; Tian, L. Metallic Nanoparticle Inks for Flexible Printed Electronics. FlexMat 2025, 2 (2), 225–283.

(35) Zhou, D.; Xiao, Z.; Zhu, L.; Liu, L.; Xu, Q. Optimized Ag NPs/Graphene Conductive Ink for High-Sensitivity Flexible Stress Sensors. Materials Today Communications 2025, 43, 111766.

(36) Jo, Y.; Jeong, S. Development of Highly Conductive Cu Conductors Using Cu Nanoparticle/Flake Inks and Instantaneous Laser Sintering Process. J. Flex. Print. Electron. 2022, 1 (1), 119–124.

(37) Shin, D.-C.; Park, G.-Y.; Go, M.-S.; Kim, B.-J. Mechanical Reliability of Cu Electrode for Flexible Electronics under Asymmetric Bending Deformations. J. Flex. Print. Electron. 2024, 3 (2), 241–247.

(38) Huang, P.-Y.; Huang, C.-Y.; Li, J.-W.; Shen, S.-Y.; Cheng, C.-C.; Chiu, C.-W.; Jeng, R.-J.; Lin, J.-J. Immobilization of Air-Stable Copper Nanoparticles on Graphene Oxide Flexible Hybrid Films for Smart Clothes. Polymers 2022, 14 (2), 237.

(39) Htwe, Y. Z. N.; Mariatti, M. Performance of Water-Based Printed Hybrid Graphene/Silver Nanoparticle Conductive Inks for Flexible Strain Sensor Applications. Synthetic Metals 2023, 300, 117495.

(40) Kaindl, R.; Gupta, T.; Blümel, A.; Pei, S.; Hou, P.-X.; Du, J.; Liu, C.; Patter, P.; Popovic, K.; Dergez, D.; Elibol, K.; Schafler, E.; Liu, J.; Eder, D.; Kieslinger, D.; Ren, W.; Hartmann, P.; Waldhauser, W.; Bayer, B. C. Aerosol Jet Printing of Graphene and Carbon Nanotube Patterns on Realistically Rugged Substrates. ACS Omega 2021, 6 (50), 34301–34313.

(41) Song, D.; Mahajan, A.; Secor, E. B.; Hersam, M. C.; Francis, L. F.; Frisbie, C. D. High-Resolution Transfer Printing of Graphene Lines for Fully Printed, Flexible Electronics. ACS Nano 2017, 11 (7), 7431–7439.
(42) Mahajan, A.; Frisbie, C. D.; Francis, L. F. Optimization of Aerosol Jet Printing for High-Resolution, High-Aspect Ratio Silver Lines. ACS Appl. Mater. Interfaces 2013, 5 (11), 4856–4864.
(43) Tran, T. S.; Dutta, N. K.; Choudhury, N. R. Graphene Inks for Printed Flexible Electronics: Graphene Dispersions, Ink Formulations, Printing Techniques and Applications. Advances in Colloid and Interface Science 2018, 261, 41–61.
(44) Zhang, L.; Liu, H.; Zhao, Y.; Sun, X.; Wen, Y.; Guo, Y.; Gao, X.; Di, C.; Yu, G.; Liu, Y. Inkjet Printing High-Resolution, Large-Area Graphene Patterns by Coffee-Ring Lithography. Advanced Materials 2012, 24 (3), 436–440.
(45) Sliz, R.; Czajkowski, J.; Fabritius, T. Taming the Coffee Ring Effect: Enhanced Thermal Control as a Method for Thin-Film Nanopatterning. Langmuir 2020, 36 (32), 9562–9570.
(46) Loh, H. A.; Graves, A. R.; Stinespring, C. D.; Sierros, K. A. Direct Ink Writing of Graphene-Based Solutions for Gas Sensing. ACS Appl. Nano Mater. 2019, 2 (7), 4104–4112.
(47) Saidina, D. S.; Mariatti, M.; Zubir, S. A.; Fontana, S.; Hérold, C. Performance of Graphene Hybrid-Based Ink for Flexible Electronics. J Mater Sci: Mater Electron 2019, 30 (22), 19906–19916.
(48) Karim, N.; Afroj, S.; Tan, S.; Novoselov, K. S.; Yeates, S. G. All Inkjet-Printed Graphene-Silver Composite Ink on Textiles for Highly Conductive Wearable Electronics Applications. Sci Rep 2019, 9 (1), 8035.
(49) Gao, Y.; Shi, W.; Wang, W.; Leng, Y.; Zhao, Y. Inkjet Printing Patterns of Highly Conductive Pristine Graphene on Flexible Substrates. Ind. Eng. Chem. Res. 2014, 53 (43), 16777–16784.
(50) Jabari, E.; Toyserkani, E. Micro-Scale Aerosol-Jet Printing of Graphene Interconnects. Carbon 2015, 91, 321–329.
(51) Guyll, B. I.; Sanford, B. L.; Pint, C. L.; Secor, E. B. Controlling Droplet Evaporation in Aerosol Jet Printing to Understand and Mitigate Overspray. Small Science 2025, 5 (7), 2500069.
(52) Gamba, L.; Diaz-Arauzo, S.; Hersam, M. C.; Secor, E. B. Aerosol Jet Printing of Phase-Inversion Graphene Inks for High-Aspect-Ratio Printed Electronics and Sensors. ACS Appl. Nano Mater. 2023, 6 (22), 21133–21140.
(53) Chen, G.; Gu, Y.; Tsang, H.; Hines, D. R.; Das, S. The Effect of Droplet Sizes on Overspray in Aerosol-Jet Printing. Adv Eng Mater 2018, 20 (8), 1701084.
(54) He, P.; Cao, J.; Ding, H.; Liu, C.; Neilson, J.; Li, Z.; Kinloch, I. A.; Derby, B. Screen-Printing of a Highly Conductive Graphene Ink for Flexible Printed Electronics. ACS Appl. Mater. Interfaces 2019, 11 (35), 32225–32234.
(55) Vasileva, F.; Popov, V.; Antonova, I.; Smagulova, S. Screen-Printed Structures from a Highly Conductive Mildly Oxidized Graphene Suspension for Flexible Electronics. Materials 2022, 15 (3), 1256.
(56) Liu, L.; Shen, Z.; Zhang, X.; Ma, H. Highly Conductive Graphene/Carbon Black Screen Printing Inks for Flexible Electronics. Journal of Colloid and Interface Science 2021, 582, 12–21.
(57) Hyun, W. J.; Secor, E. B.; Hersam, M. C.; Frisbie, C. D.; Francis, L. F. High-Resolution Patterning of Graphene by Screen Printing with a Silicon Stencil for Highly Flexible Printed Electronics. Advanced Materials 2015, 27 (1), 109–115.
(58) Ji, S.; Choi, W.; Kim, H.-Y.; Jeon, J.-W.; Cho, S.-H.; Chang, W. Fully Solution-Processable Fabrication of Multi-Layered Circuits on a Flexible Substrate Using Laser Processing. Materials 2018, 11 (2), 268.
(59) Zhou, M.; Li, Z.; Wang, Z.; Li, X.; Wang, R.; Li, H.; Zhang, H.; Sun, W.; Wang, T.; Liu, X.; Lan, H.; Zhu, X. All-Printed VIA-Free Polyimide-Based Multilayer Flexible Circuits. Journal of Materials Science & Technology 2026, 249, 131–141.
(60) Kujala, M.; Kololuoma, T.; Keskinen, J.; Lupo, D.; Mäntysalo, M.; Kraft, T. M. Bending Reliability of Screen-Printed Vias for a Flexible Energy Module. npj Flex Electron 2020, 4 (1), 24.
(61) Zhao, W.; Wang, L. Microdrilling of Through-Holes in Flexible Printed Circuits Using Picosecond Ultrashort Pulse Laser. Polymers 2018, 10 (12), 1390.
(62) Goh, G. L.; Agarwala, S.; Yeong, W. Y. Aerosol-Jet-Printed Preferentially Aligned Carbon Nanotube Twin-Lines for Printed Electronics. ACS Appl. Mater. Interfaces 2019, 11 (46), 43719–43730.
(63) Jabari, E.; Toyserkani, E. Aerosol-Jet Printing of Highly Flexible and Conductive

Graphene/Silver Patterns. Materials Letters 2016, 174, 40–43.
(64) Babatain, W.; Park, C.; Ishii, H.; Gershenfeld, N. Laser-Enabled Fabrication of Flexible Printed Electronics with Integrated Functional Devices. Advanced Science 2025, 12 (20), 2415272.
(65) Ye, R.; James, D. K.; Tour, J. M. Laser-Induced Graphene. Acc. Chem. Res. 2018, 51 (7), 1609–1620.
(66) Rektor, A.; Eixenberger, J.; Valayil Varghese, T.; Cummings, B.; Curtis, M.; Mckibben, N.; Timler, J.; Estrada, D. Electroless Plating of Copper on Laser-Induced Graphene for Flexible Hybrid Electronic Applications. Adv Materials Technologies 2025, 10 (9), 2401901.
(67) Yoon, S. J.; Min, J.; Ko, S. H. Fabrication of Flexible Printed Electronic Using Selective Laser Sintering. J. Flex. Print. Electron. 2022, 1 (2), 189–199.
(68) Wang, H.; Zhao, Z.; Liu, P.; Guo, X. Laser-Induced Graphene Based Flexible Electronic Devices. Biosensors 2022, 12 (2), 55.
(69) Pandhi, T.; Kreit, E.; Aga, R.; Fujimoto, K.; Sharbati, M. T.; Khademi, S.; Chang, A. N.; Xiong, F.; Koehne, J.; Heckman, E. M.; Estrada, D. Electrical Transport and Power Dissipation in Aerosol-Jet-Printed Graphene Interconnects. Sci Rep 2018, 8 (1), 10842.
(70) Heaton, C. E. D.; Austin, J. S.; Ruer, L.; Cottam, N. D.; Wang, F.; He, Y.; Rance, G. A.; Rose, F. R. A. J.; Wildman, R. D.; Hague, R. J. M.; Makarovsky, O.; Turyanska, L. Photonic Annealing of Inkjet Printed Graphene for Stretchable Wearable Healthcare Monitoring Devices. Adv Materials Technologies 2025, 10 (21), e00913.
(71) Jang, Y.-R.; Joo, S.-J.; Chu, J.-H.; Uhm, H.-J.; Park, J.-W.; Ryu, C.-H.; Yu, M.-H.; Kim, H.-S. A Review on Intense Pulsed Light Sintering Technologies for Conductive Electrodes in Printed Electronics. Int. J. of Precis. Eng. and Manuf.-Green Tech. 2021, 8 (1), 327–363.
(72) Secor, E. B.; Gao, T. Z.; Dos Santos, M. H.; Wallace, S. G.; Putz, K. W.; Hersam, M. C. Combustion-Assisted Photonic Annealing of Printable Graphene Inks via Exothermic Binders. ACS Appl. Mater. Interfaces 2017, 9 (35), 29418–29423.
(73) Huang, X.; Leng, T.; Zhu, M.; Zhang, X.; Chen, J.; Chang, K.; Aqeeli, M.; Geim, A. K.; Novoselov, K. S.; Hu, Z. Highly Flexible and Conductive Printed Graphene for Wireless Wearable Communications Applications. Sci Rep 2015, 5 (1), 18298.
(74) Zhang, K.; Surana, M.; Yaacoub, J.; Tawfick, S. Ultrathin Damage-Tolerant Flexible Metal Interconnects Reinforced by in-Situ Graphene Synthesis. npj Flex Electron 2024, 8 (1), 16.
(75) Won, P.; Park, J. J.; Lee, T.; Ha, I.; Han, S.; Choi, M.; Lee, J.; Hong, S.; Cho, K.-J.; Ko, S. H. Stretchable and Transparent Kirigami Conductor of Nanowire Percolation Network for Electronic Skin Applications. Nano Lett. 2019, 19 (9), 6087–6096.
(76) Yoo, H.; Lee, S.-H.; Kim, S.-M.; Jo, J.-H.; Kim, J.-Y. Research Progress in Flexible and Stretchable Encapsulation Materials for Electronics. J. Flex. Print. Electron. 2025, 4 (1), 15–30.
(77) Kwon, Y.-T.; Kim, Y.-S.; Kwon, S.; Mahmood, M.; Lim, H.-R.; Park, S.-W.; Kang, S.-O.; Choi, J. J.; Herbert, R.; Jang, Y. C.; Choa, Y.-H.; Yeo, W.-H. All-Printed Nanomembrane Wireless Bioelectronics Using a Biocompatible Solderable Graphene for Multimodal Human-Machine Interfaces. Nat Commun 2020, 11 (1), 3450.